

Master Thesis

Master's Degree in Smart Electrical Networks and Systems
Engineering

Design of a Unified Power Quality Conditioner for a Distribution System Application

July 2023

Author: Titouan Delorme

Supervisors: Eduardo Prieto Araujo
Josep Fanals i Batllori



Escola Tècnica Superior
d'Enginyeria Industrial de Barcelona



Abstract

A large trend observed recently in power systems is the introduction of solar photovoltaic in the distribution grid. This poses certain issues for the distribution system operators in particular pertaining to the voltage regulation of the grid, as solar introduces overvoltages and voltage imbalances at the connection point. Some new power electronics-based methods are being investigated currently to tackle this particular problem.

The work captured in this thesis is the design of one of these power electronics-based methods, the unified power quality conditioner, which is a combined series and shunt device. Due to the expensive nature of the device, there is a need to provide a small sizing use case for this method. The work develops tools helpful to complete this design. These include a dynamic model with phase-independent voltage correction and a static model which mimics the steady state behavior of the controllers in the dynamic model but computes much faster. These tools are applied to a design based on data from a sample distribution grid in the south of Spain encountering voltage regulation issues. This work is conducted in collaboration with TeknoCEA, a company specializing in power converters.

Resumen

Una gran tendencia observada recientemente en los sistemas de energía es la introducción de la energía solar fotovoltaica en la red de distribución. Esto plantea ciertos problemas para los operadores del sistema de distribución, particularmente en relación con la regulación de la tensión de la red, ya que la energía solar introduce sobretensiones y desequilibrios de tensión en el punto de conexión. Actualmente se están investigando algunos nuevos métodos basados la electrónica de potencia para abordar este problema.

El trabajo capturado de esta tesis es el diseño de uno de estos métodos basados en electrónica de potencia, el unified power quality conditioner, que es un dispositivo combinado en serie y en paralelo. Debido a la naturaleza costosa del dispositivo, existe la necesidad de proporcionar un caso de uso de tamaño pequeño para este método. El trabajo desarrolla herramientas útiles para completar este diseño. Estos incluyen un modelo dinámico con corrección de voltaje independiente en cada fase y un modelo estático que imita el comportamiento de estado estacionario de los controladores del modelo dinámico pero que calcula mucho más rápido. Estas herramientas se aplican a un diseño basado en datos de una red de distribución de muestra en el sur de España que enfrenta problemas de regulación de voltaje. Este trabajo se realiza en colaboración con TeknoCEA, empresa especializada en convertidores de potencia.

Resum

Una tendència notable que s'observa en l'evolució dels sistemes elèctrics de potència és la introducció de plantes solars fotovoltaïques a nivell de distribució. Aquest fet comporta certa problemàtica als operadors de les xarxes de distribució, particularment pel que fa a la regulació de voltatge atès que la fotovoltaica pot produir sobretensions i desequilibris. Nous equips basats en electrònica de potència han emergit per atacar aquest problema.

Aquest projecte tracta sobre el disseny d'un d'aquests equips d'electrònica de potència, anomenat UPQC per les seves sigles en anglès (Unified Power Quality Conditioner). Aquest dispositiu sorgeix de la combinació d'un convertidor en sèrie i un en paral·lel. Degut a la seva naturalesa costosa en temes econòmics, hi ha la necessitat de precisar en el seu dimensionament. En tal sentit, aquesta tesi desenvolupa eines per dissenyar-lo. Així, s'inclou un model dinàmic amb correcció de voltatge a cada una de les fases, i un model estàtic que permet capturar l'operació en règim permanent i reduir el temps de càlcul. Aquestes eines s'han aplicat a un disseny basat en dades recollides d'una xarxa de distribució del sud d'Espanya on s'experimenten problemes a l'hora de regular els voltatges. La feina d'aquest projecte s'ha desenvolupat en col·laboració amb TeknoCEA, una companyia especialitzada en el disseny de convertidors de potència.

Contents

Glossary	14
Preface	17
1 Introduction	19
1.1 Background	19
1.2 Objectives	20
1.3 Outline	20
2 Project Definition	23
2.1 Introduction	23
2.2 Sample System	23
2.3 UPQC Circuit	24
2.4 Project Goal	25
2.5 Design Methodology	25
3 Dynamic Model	27
3.1 Simulation Overview	27
3.2 PLL Circuit and Reference Generator	28
3.3 Series Controller	29
3.4 Shunt Controller	31
4 Static Model	33
4.1 Single-Phase	33
4.1.1 Equivalent Circuit	33
4.1.2 Variables	34
4.1.3 Equations	36
4.1.4 Voltage Limit	38
4.1.5 Workflow	38
4.2 Three-Phase	39
4.2.1 Equivalent Model	39
4.2.2 Variables	39
4.2.3 Equations	40
5 Validation	43
5.1 Dynamic	43
5.2 Static	46
6 Design and Results	59
6.1 Design Decisions	59

6.1.1	Filter Sizing	59
6.1.2	DC Link Capacitor Sizing	59
6.1.3	Transformer Turns Ratio	59
6.1.4	Series and Shunt Converter Sizing	60
6.2	Results with Sample System	60
7	Conclusion	69
7.1	Contributions	69
7.2	Future work	69
Acknowledgments		71
A	Environmental, Social, and Gender Impact	73
A.1	Integration of Renewable Energy and Removal of Fossil Fuel Generators	73
A.2	Social Impact of Outage Prevention	73
B	Time Planning	75
C	Budget	77
C.1	Equipment	77
C.2	Human resources	77
C.3	Total budget	77
Bibliography		79

List of Figures

2.1	Voltage Distribution of Line 1 of the Sample System.	23
2.2	Voltage Distribution of Line 2 of the Sample System.	23
2.3	Voltage Distribution of Line 3 of the Sample System.	23
2.4	Voltage Distribution of Line 4 of the Sample System.	23
2.5	Voltage Distribution of Line 5 of the Sample System.	23
2.6	Voltage Distribution of Line 6 of the Sample System.	23
2.7	Voltage Distribution of Line 7 of the Sample System.	24
2.8	UPQC Circuit.	24
2.9	Active Power Flow in UPQC during an Ovvervoltage.	25
2.10	Active Power Flow in UPQC during an Undervoltage.	25
3.1	Overall Controller Block Diagram.	27
3.2	Average Model Representation of a Three-Phase Inverter. Adapted from [44].	28
3.3	Block Diagram of PLL Circuit.	28
3.4	Block Diagram of PSVD and Reference Generator.	29
3.5	Block Diagram of Series Controller.	30
3.6	Block Diagram of Series Voltage Controller.	30
3.7	Block Diagram of Series Current Controller.	31
3.8	Block Diagram of SOGI.	31
3.9	Block Diagram of Shunt Controller.	32
3.10	Block Diagram of Shunt Current Controller.	32
4.1	UPQC Simplified Model.	33
4.2	Workflow of Single Phase Static Model.	38
5.1	Load and Source Voltage Magnitude with Sweep of Grid Voltages from 1.1 to 0.9 p.u..	43
5.2	Series and Shunt Converter Active Power with Sweep of Grid Voltages from 1.1 to 0.9 p.u..	43
5.3	Series and Shunt Converter Reactive Power with Sweep of Grid Voltages from 1.1 to 0.9 p.u..	44
5.4	DC Voltage with Sweep of Grid Voltages from 1.1 to 0.9 p.u..	44
5.5	Load and Source Voltage Magnitude with Sweep of Grid Voltages from 1.1 to 0.9 p.u. and Voltage Correction Limit of 20 V.	44
5.6	Series and Shunt Converter Active Power with Sweep of Grid Voltages from 1.1 to 0.9 p.u. and Voltage Correction Limit of 20 V.	45
5.7	Series and Shunt Converter Reactive Power with Sweep of Grid Voltages from 1.1 to 0.9 p.u. and Voltage Correction Limit of 20 V.	45
5.8	DC Voltage with Sweep of Grid Voltages from 1.1 to 0.9 p.u. and Voltage Correction Limit of 20 V.	45

5.9	Static Model Validation with a Load Power Factor pf=1 and Transformer Ratio of $N_T=20$.	46
5.10	Static Model Validation with an Inductive Load Power Factor pf=0.8 and Transformer Ratio of $N_T=20$.	48
5.11	Static Model Validation with an Capacitive Load Power Factor pf=0.8 and Transformer Ratio of $N_T=20$.	49
5.12	Static Model Validation with a Voltage Limit of 0.05p.u., a Load Power Factor pf=1 and Transformer Ratio of $N_T=20$.	50
5.13	Static Model Validation with a Voltage Limit of 0.05p.u., an Inductive Load Power Factor pf=0.8 and Transformer Ratio of $N_T=20$.	51
5.14	Static Model Validation with a Voltage Limit of 0.05p.u., a Capacitive Load Power Factor pf=0.8 and Transformer Ratio of $N_T=20$.	52
5.15	Three Phase Static Model Validation with a Load Power Factor pf=1 and Transformer Ratio $N_T=20$.	53
5.16	Three Phase Static Model Validation with an Inductive Load Power Factor pf=0.8 and Transformer Ratio of $N_T=20$.	54
5.17	Three Phase Static Model Validation with a Capacitive Load Power Factor pf=0.8 and Transformer Ratio $N_T=20$.	55
5.18	Three Phase Static Model Validation with a Voltage Limit of 0.05p.u., Load Power Factor pf=1 and Transformer Ratio $N_T=20$.	56
5.19	Three Phase Static Model Validation with a Voltage Limit of 0.05p.u., an Inductive Load Power Factor pf=0.8 and Transformer Ratio of $N_T=20$.	57
5.20	Three Phase Static Model Validation with a Voltage Limit of 0.05p.u.,a Capacitive Load Power Factor pf=0.8 and transformer ratio $N_T=20$.	58
6.1	Series Apparent Power with Sweep of Transformer Ratios and Three Different Load Power Factors.	60
6.2	Sample Day in May for Line 1 of the Studied System.	61
6.3	Sample Day of the UPQC Static Model from a Day in May with Voltage Limit Set to 99.9% Case.	62
6.4	Sample Day of the UPQC Static Model from a Day in May with Voltage Limit Set to 99% Case.	63
6.5	Sample Day of the UPQC Static Model from a Day in May with Voltage Limit Set to 95% Case.	64
6.6	Sample Day in November for Line 1 of the Studied System.	64
6.7	Sample Day of the UPQC Static Model from a Day in November with Voltage Limit Set to 99.9% Case.	65
6.8	Sample Day of the UPQC Static Model from a Day in November with Voltage Limit Set to 99% Case.	66

6.9	Sample Day of the UPQC Static Model from a Day in November with Voltage Limit Set to 95% Case.	67
6.10	Sample Day of the UPQC Static Model from a Day in November with Voltage Limit Set to 95% Case.	67
B.1	Gantt Diagram Illustrating the Project Evolution.	75

List of Tables

4.1 Single Phase Static Model Unknown Variables.	35
4.2 Three Phase Static Model Unknown Variables.	39
6.1 Test Voltage Limits for Each Sample System Line and Corresponding Converter Power.	60
C.1 Equipment Costs.	77
C.2 Human Resources Costs.	77
C.3 Total Budget of the Thesis.	77

Glossary

Symbols

C	Capacitance
C_f	Shunt filter capacitance
C_s	Corrected series filter capacitance
C'_s	Series filter capacitance
f_c	Cutoff frequency
i_c	Shunt current
i_{cs}	Series converter current
i_{cf}	Shunt Converter current
i_L	Load current
i_s	Source Voltage
L	Inductance
L_f	Shunt filter inductance
L_l	Line inductance
L_s	Corrected series filter inductance
L'_s	Series filter inductance
N_T	Series transformer turns ratio
P	Active power
pf	Power factor
P_L	Load active power
Q	Reactive power
Q_L	Load reactive power
Q_{sh}	Shunt converter reactive power
R_f	Shunt filter resistance
R_l	Line resistance
R_s	Corrected series filter resistance
R'_s	Series filter resistance
\underline{S}_L	Load apparent power
u_c	Series correction voltage
$u_{c,lim}$	Voltage correction limit
u_{cs}	Series converter voltage
u_{cf}	Shunt Converter voltage
u_{DC}	DC Link Voltage
u_G	Grid voltage
u_L	Load voltage
u_s	Source voltage
x_i	Dummy variable

\underline{x}_i	Complex dummy variable
$ \underline{x}_i $	Magnitude of dummy variable
$x_{i,\mathbb{R}}$	Real component of dummy variable
$x_{i,\mathbb{I}}$	Imaginary component of dummy variable
$x_{i,\alpha}$	Alpha component of dummy variable
$x_{i,\beta}$	Beta component of dummy variable
$x_{i,a}$	Phase a component of dummy variable
$x_{i,b}$	Phase b component of dummy variable
$x_{i,c}$	Phase c component of dummy variable
θ_{sys}	System angle
ω_{sys}	System frequency

Acronyms

AC	Alternating Current
CITCEA	Centre d'Innovació Tecnològica en Convertidors Estàtics i Accionaments
DC	Direct Current
DSTATCOM	Distribution Static Synchronous Compensator
DVR	Dynamic Voltage Regulator
FACTS	Flexible AC Transmission Systems
IEEE	Institute of Electrical and Electronics Engineers
LC	Inductive and Capacitive Low Pass Filter
OLTC	On Load Tap Changer
PI	Proportional Integral
PLL	Phase Locked Loop
PSVD	Positive Sequence Voltage Detector
PV	Photovoltaic
RMS	Root Mean Square
SOGI	Second Order Generalized Integrator
UPC	Universitat Politècnica de Catalunya
UPFC	Unified Power Flow Controller
UPQC	Unified Power Quality Conditioner
VRE	Variable Renewable Energy

Preface

Traditional power systems have many techniques to provide voltage regulation to the grid. The specificities of these techniques are well known to the community and little innovation is required to regulate voltage in the traditional grid. However, the introduction of renewable sources, particularly PV, is rendering many older technologies obsolete for faster applications required in modern power systems. Consequently, new techniques for voltage regulation are being developed to fit the needs of the modern system.

An issue that the new techniques face is that they are more expensive than traditional techniques. Traditional techniques are very mature and quite optimized. It is thus important to keep pushing new voltage regulation methods towards maturity so they can compete with the traditional methods economically. Without this, the full integration of renewables will be pushed back further and further.

The work developed at eRoots Analytics as part of a consulting project for Teknocea attempts to provide more mature tools to aid in the design of one of these new solutions, the UPQC. The methods and tools developed in this project are set to become a contribution to further new methods of voltage regulation.

1 Introduction

1.1 Background

To ensure the sustainability of the planet in the future, there is a strong need to curb environmental pollution in the coming years [1]. With the Paris Climate Accords in 2015, the goal was set to limit the global temperature increase by 2°C [2]. One of the proposed solutions to accomplish this goal is replacing the existing fossil fuel generation with a large-scale renewable energy supply in the current power system [3]. This transition poses some new problems for the power system. These problems include but are not limited to loss of inertia in the system [4, 5], reverse power flows [5–7], low fault currents [5, 8], larger voltage variation [5, 7], and unbalances [9]. As such, the utility industry is subjected to a paradigm shift towards a new customer-centric reality, which encompasses infrastructure, organizational, business, and regulatory aspects [5].

At the distribution level, larger and quicker voltage variation and imbalances are specifically related to the intermittent nature of VRE sources, particularly solar PV [10–12]. More specifically, the voltage variations caused by PV tends towards overvoltage [13]. Voltage variation and imbalances also occur in traditional power systems under certain conditions albeit to a lesser extent. Voltage imbalances occur when there is an uneven distribution of single-phase loads in the three phases, or a synchronous machine is overloaded in one of its phases [14]. Overvoltages are the result of lightning strikes or sudden switches in the network but are rarely found at the distribution level in traditional systems [15]. These phenomena have detrimental effects on the network as a whole. Overvoltages stress the insulation of the power system and can thus reduce the usable lifetime of components such as power lines and transformers [16, 17]. They may thus cause the PV to be disconnected [18]. Additionally, it will reduce the hosting capacity of the network [5]. Voltage imbalances may amplify the presence of harmonics in other power electronics-based devices in the system and cause the system to become unstable [19]. They also cause motor damage due to excess heat [20].

Some solutions already exist to combat these issues in the grid. The most comprehensive method is to reconfigure the low-voltage network. In particular, increasing the cross-section of the feeder has been shown to greatly improve the imbalances and make voltage regulation methods more effective [9]. However, this method is seldom employed due to the high costs involved [21]. Another traditional method is the use of OLTCs, although their response is generally too slow for the quicker voltage variation present with PV [9, 22]. Similarly, the use of switched capacitor banks is common in traditional systems but is less useful in this scenario because exact reactive power is unable to be provided [9, 23]. Some emerging mitigation methods are also being investigated. Firstly, the injection of reactive power from solar PV inverters to stabilize voltage has been investigated in various pieces of literature [24–26]. The obstacle to this solution is not a technical but rather a regulatory one, as decentralized voltage regulation is still not

allowed by most standards [27–29]. The PV inverter solution may also be used in coordination with grid equipment. There is particular attention paid in the literature to combining OLTCs with PV inverters connected in series [12, 21]. Secondly, two forms of power electronics-based compensators are investigated as a solution, particularly for voltage imbalances. The series connected DVR [30, 31] and the shunt connection DSTATCOM [32, 33] are shown to both be useful to correct imbalances, although a comparison of both solutions has shown DSTATCOMs to be more effective at the cost of larger sizing of components [34]. Finally, the UPQC, also referred to as UPFC in literature and which combines the series and shunt-connected converters is investigated in [35, 36], but is more expensive than the other solution due to the presence of more components [37] and thus has not reached large scale implementation as of yet.

1.2 Objectives

Considering the state of the art, the goals of the thesis are as follows:

- To analyze the effect of PV connection on the voltage variation of the distribution grid. In particular, the voltage data of a sample grid with PV connection is studied.
- To develop phase-independent series voltage control of a UPQC to manage unbalanced voltage variation in a distribution grid with PV connection. Control diagrams of the series control, shunt control, and reference generation are provided.
- To develop and validate a static model of the UPQC behavior outlined in the controller to aid the sizing of UPQC components.
- To employ the tools described above in the lowest cost sizing of a UPQC to fulfill voltage correction requirements.

1.3 Outline

The structure of the thesis is shown below:

- Chapter 2 overviews the system studied in the project and analyses the voltage distribution at the PCC. The UPQC is introduced and the goals for the converter design are presented. The design methodology is then outlined.
- Chapter 3 outlines the dynamic model of the UPQC based on the average model representation of the converter. The connections of each terminal of the UPQC are specified. In addition, the controller goals and diagrams of the UPQC are presented.
- Chapter 4 outlines both a single-phase and three-phase equivalent static representation of the converter. Throughout this process, an equivalent circuit, assumptions about the circuit, and a system of equations and unknowns are outlined for each case.

- Chapter 5 is centered around the validation of both models. First, different scenarios of the dynamic model are shown to ensure control objectives are fulfilled. Second, the static model is run under similar scenarios to confirm the results line up with the dynamic model. The results and potential limitations are also discussed.
- Chapter 6 contains the final design decisions for the UPQC. Subsequently, sample day profiles for the UPQC response are presented and discussed.
- Chapter 7 shares the conclusions of the project and discusses further steps that can be taken.

2 Project Definition

2.1 Introduction

The objective of this project is to design a UPQC with minimum sizing to fulfill the voltage correction of a given system. The project is conducted in conjunction with a company named TeknoCEA. The system in question is a distribution system in the southern part of Spain with PV connected and some voltage issues. Actual data for the grid voltage and load power is provided for the second half of 2022 and the first half of 2023 and is provided with a resolution of 5 minutes.

2.2 Sample System

The system used for this application is a remote distribution system with a solar power plant attached to the grid side near the distribution transformer. The distribution system has 7 different lines with connections from the solar plant. The phase-by-phase connection of the solar plant causes voltage imbalances and variations on the consumer side of the distribution grid. This variation is generally contained between 0.98 and 1.05 p.u. and is never lower than 0.95 p.u. nor higher than 1.10 p.u. As such, the voltage variation tends towards overvoltage, which is in line with trends observed in the literature [13]. The voltage distribution over a full year of all 7 lines is shown in Figs. 2.1-2.7.

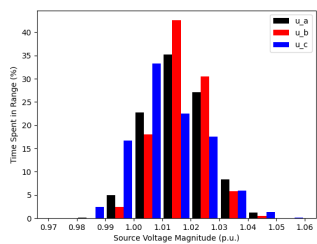


Figure 2.1: Voltage Distribution of Line 1 of the Sample System.

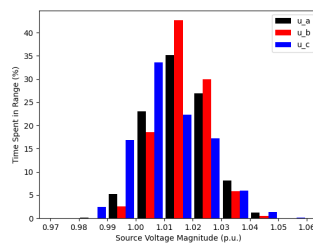


Figure 2.2: Voltage Distribution of Line 2 of the Sample System.

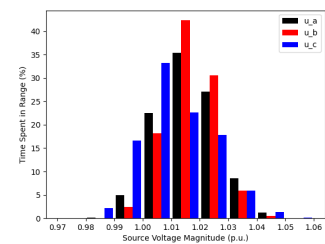


Figure 2.3: Voltage Distribution of Line 3 of the Sample System.

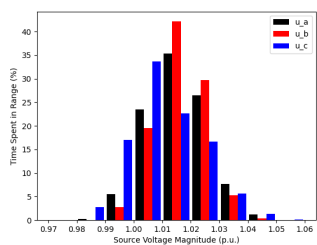


Figure 2.4: Voltage Distribution of Line 4 of the Sample System.

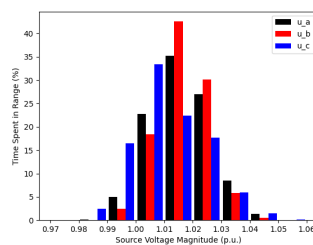


Figure 2.5: Voltage Distribution of Line 5 of the Sample System.

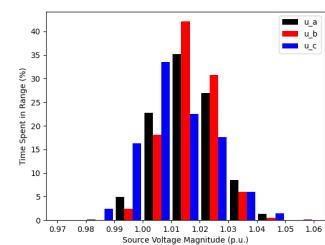


Figure 2.6: Voltage Distribution of Line 6 of the Sample System.

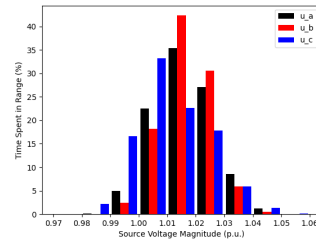


Figure 2.7: Voltage Distribution of Line 7 of the Sample System.

2.3 UPQC Circuit

A unified power quality conditioner (UPQC), also known as a universal active filter, is a multi-function power conditioner. Along with correcting voltage variations and imbalances, it can be used to compensate for disturbances in the power supply [38, 39], correct voltage fluctuation [40, 41], and prevent load current harmonics from entering the grid [42]. It is thus often described as the most versatile FACTS device [9].

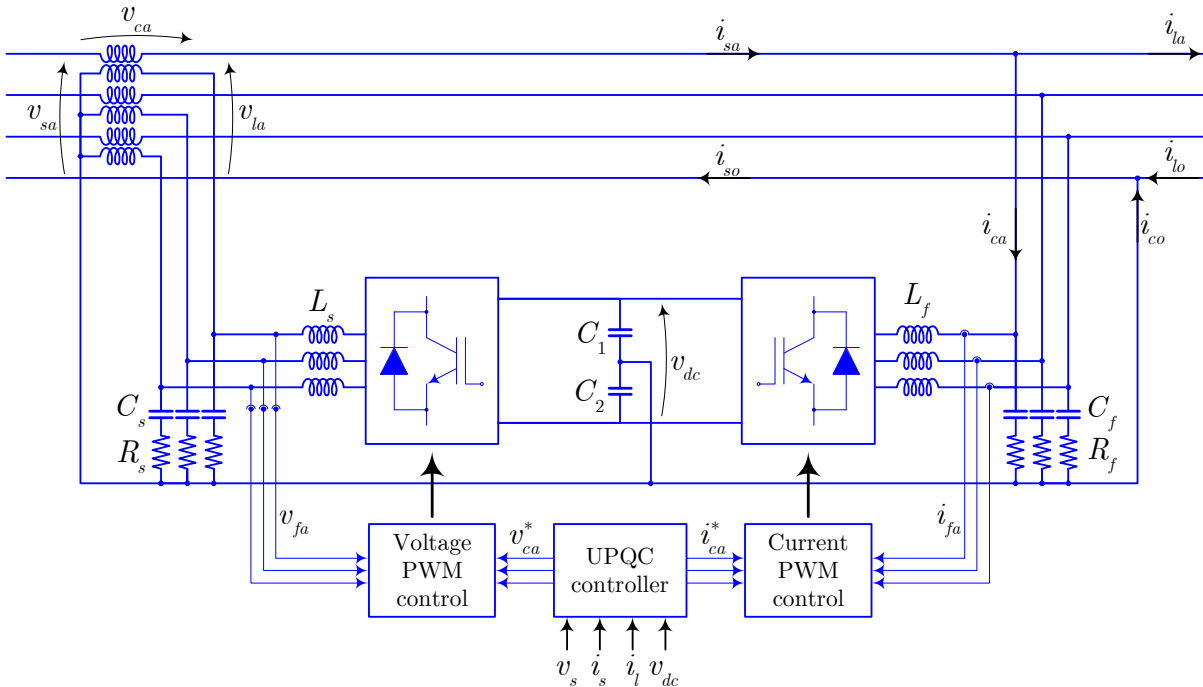


Figure 2.8: UPQC Circuit.

A UPQC contains back-to-back voltage source converters that can be connected in single-phase, three-phase three-wire, and three-phase four-wire configurations. his application uses the three phase four wire configuration. One of the converters is connected in series between the source and the critical load at the PCC through a transformer and operates as a voltage-source inverter. The other converter is connected in shunt directly at the PCC and operates as a current source inverter. These converters are named the series converter and shunt converter respectively [43].

The full circuit of the UPQC for the studied application is shown below in Fig. 2.8. Diagrams showing the active power flow in the UPQC during over and undervoltages are also displayed in Figs. 2.9-2.10.

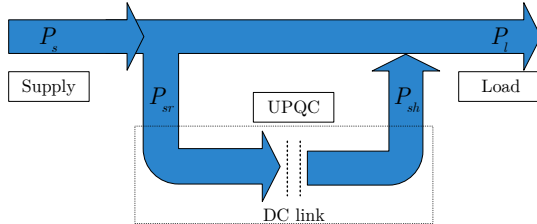


Figure 2.9: Active Power Flow in UPQC during an Overvoltage.

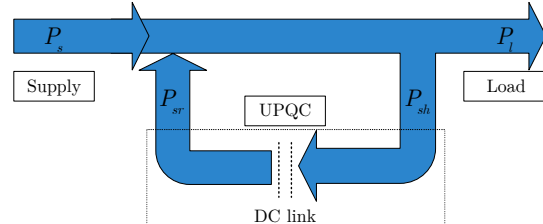


Figure 2.10: Active Power Flow in UPQC during an Undervoltage.

2.4 Project Goal

The goal of this project is to replace the current voltage support methods in the distribution systems with a UPQC. However, a fully rated UPQC is still not a viable economic option to provide this service. Instead, both converters are sized such that they will only correct a certain percentage of the voltage variation. Three difference scenarios will be trailed, with 99.9%, 99%, and 95% of the voltage deviation corrected in each case respectively. As an additional method to reduce sizing, significant voltage correction will be made only in the fundamental component of the voltage. Reduction of harmonics is outside of the scope of this design.

2.5 Design Methodology

The design of this converter will be completed using a three step approach with validation at every step. The first step is to develop a full dynamic model of the UPQC. The second is to develop a static model to model the steady state behavior of the UPQC, which will be validated with the behaviour of the dynamic model. Finally, the final design parameters of the UPQC will be chosen using a comparison of the static model under different cases.

3 Dynamic Model

3.1 Simulation Overview

To develop a static model which can be optimized, there must first be a dynamic reference to compare the steady state values against. As such, the first model developed for this project was a full dynamic simulation of the UPQC circuit using Simulink. This dynamic model follows the circuit shown in Fig. 2.8. In order to simplify the simulation, the average model representation is used for both the series and shunt converter. This simplification involves replacing the switching elements of the inverter with voltage sources and placing a dependent current source on the DC side to compensate for the active power entering and exiting the converter from the DC side. A diagram of the equivalent model representation is shown in Fig. 3.2. The dynamic model was built in MATLAB Simulink with the aid of the Simscape specialized power systems toolbox. The model along with all the control is implemented in discrete time with a time step of 20 μs .

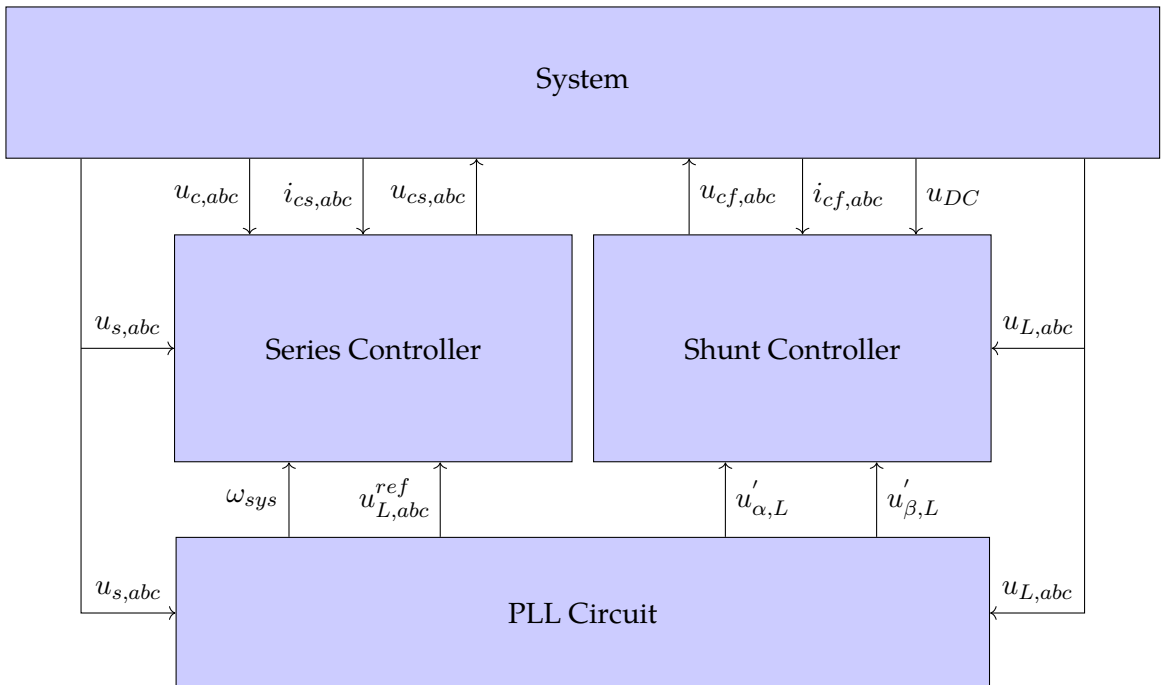


Figure 3.1: Overall Controller Block Diagram.

In terms of external connections to the actual UPQC circuit, the left, or series, side is connected to a Thévenin grid equivalent. meanwhile, the right, or shunt, side is connected to a load which can absorb both active and reactive power. In addition to the total physical circuit, there is control that is split into three blocks, a PLL circuit with reference generator, a controller for the series converter and a controller for the shunt converter. An overall control diagram outlining these three controllers is shown in Fig. 3.1, with inputs and outputs between the system and the controllers outlined.

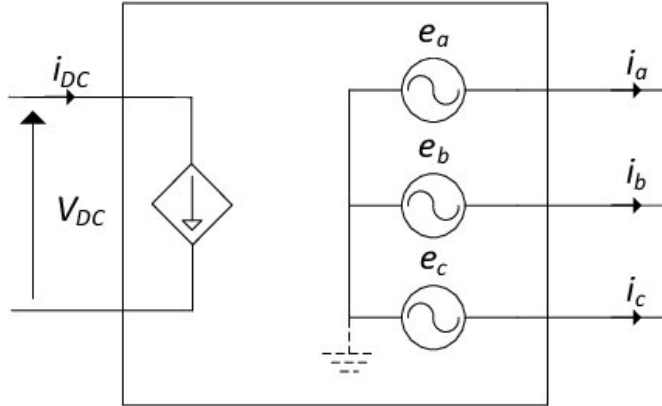


Figure 3.2: Average Model Representation of a Three-Phase Inverter. Adapted from [44].

3.2 PLL Circuit and Reference Generator

The reference generator is the base of the control system, as it provides important inputs to both the series and shunt controller. At its center is the PLL circuit. The PLL circuit uses the load voltage v_L as a reference to obtain the load voltage angle and by extension the frequency of the system. The logic used for the PLL is based on the PLL used in a more complete UPQC application [45]. It is shown in Fig. 3.3.

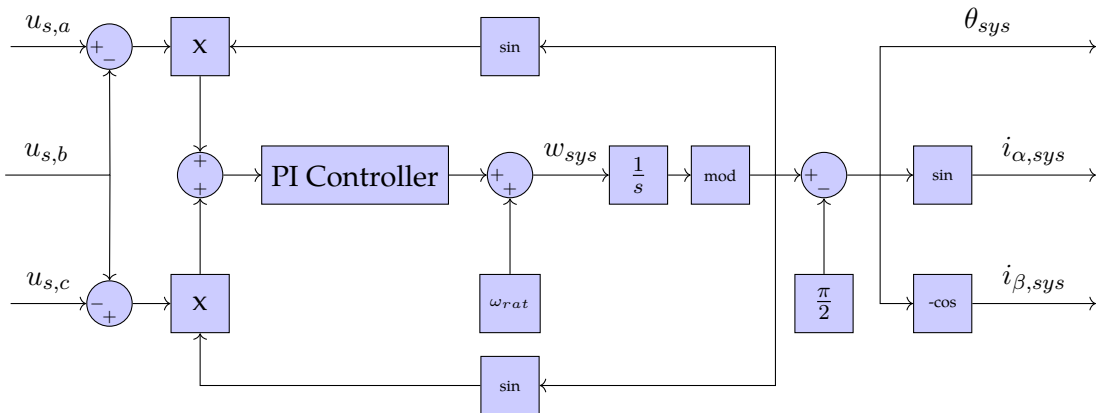


Figure 3.3: Block Diagram of PLL Circuit.

Four outputs are then generated from the PLL, the load voltage angle and frequency, and the Clarke components of a current with a magnitude of 1 in line with the voltage angle. The Clarke components are then fed into a positive sequence voltage detector (PSVD), shown in Fig. 3.4, to get the positive sequence component of the load voltage. The positive sequence voltage detector functions by first extracting a mock active and reactive power value for the system. The first step of this process is using a Clarke transform on the measured load voltage as in (3.1). Then mock active and reactive powers are generated using the measured load voltage and unit system current from the PLL as shown in (3.2). These power calculations are then fed through a low pass filter to remove all components but the fundamental. Finally, using the method shown in

(3.3), the positive sequence components of the load voltage can be extracted. These positive sequence components of the voltage are then fed into the shunt controller. In addition, the grid angle is then fed to generate the reference desired voltage at the load, and the frequency is fed directly to the series controller. The load voltage reference is set accordingly (3.4).

$$\begin{bmatrix} u_{\alpha,L} \\ u_{\beta,L} \end{bmatrix} = \sqrt{\frac{2}{3}} \begin{bmatrix} 1 & -\frac{1}{2} & -\frac{1}{2} \\ 0 & \frac{\sqrt{3}}{2} & -\frac{\sqrt{3}}{2} \end{bmatrix} \begin{bmatrix} u_{L,a} \\ u_{L,b} \\ u_{L,c} \end{bmatrix} \quad (3.1)$$

$$\begin{bmatrix} P' \\ Q' \end{bmatrix} = \begin{bmatrix} i_{\alpha,sys} & i_{\beta,sys} \\ -i_{\beta,sys} & i_{\alpha,sys} \end{bmatrix} \begin{bmatrix} u_{\alpha,L} \\ u_{\beta,L} \end{bmatrix} \quad (3.2)$$

$$\begin{bmatrix} u'_{\alpha,L} \\ u'_{\beta,L} \end{bmatrix} = \frac{1}{i_{\alpha,sys}^2 + i_{\beta,sys}^2} \begin{bmatrix} i_{\alpha,sys} & -i_{\beta,sys} \\ i_{\beta,sys} & i_{\alpha,sys} \end{bmatrix} \begin{bmatrix} \bar{P}' \\ \bar{Q}' \end{bmatrix} \quad (3.3)$$

$$\begin{bmatrix} u_{L,a}^{ref} \\ u_{L,b}^{ref} \\ u_{L,c}^{ref} \end{bmatrix} = \begin{bmatrix} u_L^{nom} \sin(\theta_{ref}) \\ u_L^{nom} \sin(\theta_{ref} - \frac{2\pi}{3}) \\ u_L^{nom} \sin(\theta_{ref} + \frac{2\pi}{3}) \end{bmatrix} \quad (3.4)$$

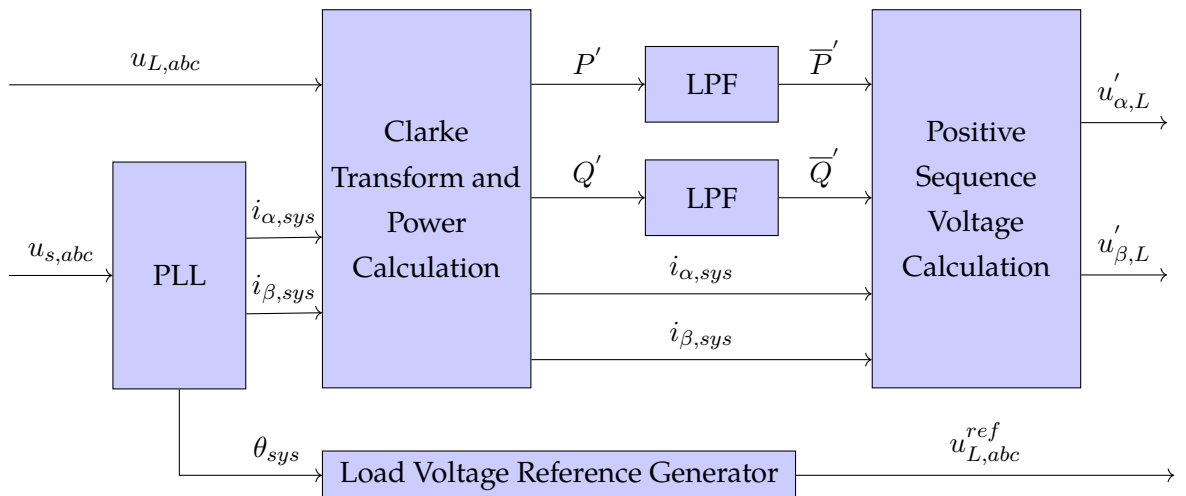


Figure 3.4: Block Diagram of PSVD and Reference Generator.

3.3 Series Controller

The series controller has the goal of keeping the individual phase voltages at the nominal voltage. However, as outlined in the project goals, the maximum correction possible is a specified value $u_{c,lim}$. As such, the series controller must also implement a voltage limit to fulfill this condition.

If the voltage sag or swell is larger than this $u_{c,lim}$ limit, the series converter will thus correct exactly $u_{c,lim}$.

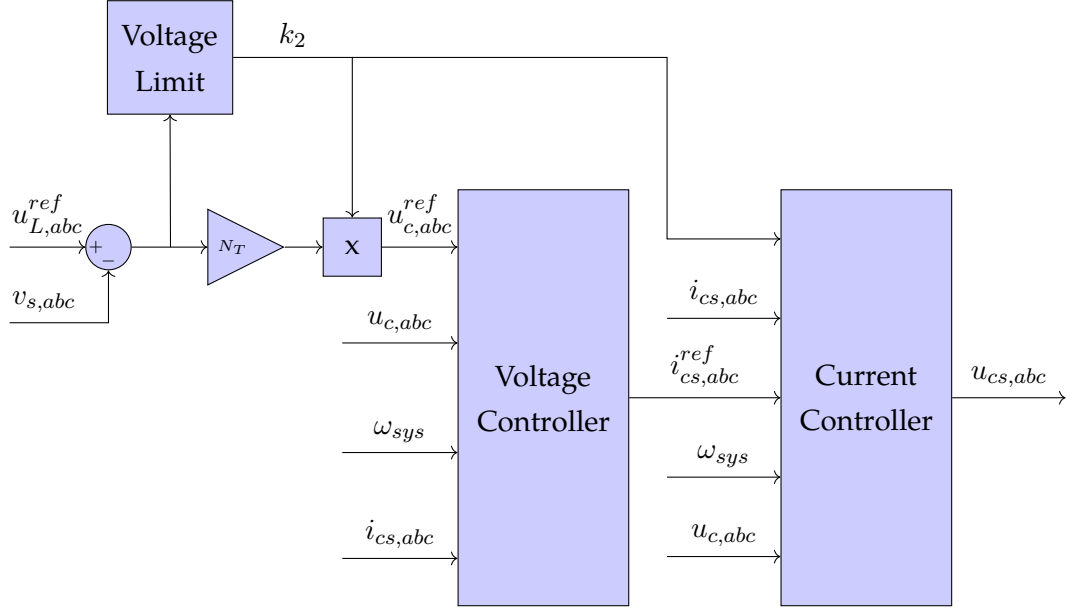


Figure 3.5: Block Diagram of Series Controller.

$$\forall i \in a, b, c \quad k_{2,i} = \begin{cases} 1, & \text{if } \text{RMS}(u_{L,i}^{ref} - u_{s,i}) \leq u_{c,nom} \\ \frac{v_{c,nom}}{\text{RMS}(u_{L,i}^{ref} - u_{s,i})}, & \text{if } \text{RMS}(u_{L,i}^{ref} - u_{s,i}) > u_{c,nom} \end{cases} \quad (3.5)$$

The controller is composed of two cascaded controllers for current and voltage control of the series controller. The overview control of the series controller is outlined in Fig. 3.5. The reference for the series voltage correction is computed by subtracting the measured source voltage from the load voltage reference from the reference generator. This reference is then multiplied by the transformer turns ratio and a factor from the voltage limit computation to make sure the series voltage correction is no more than $u_{c,lim}$. The voltage limit factor is computed following (3.5).

Both the voltage and current blocks are identical except for the voltage limit multiplier present in the current controller. The general structure of both controllers is a proportional resonant

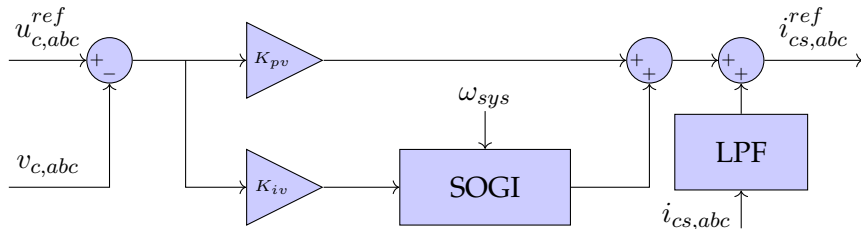


Figure 3.6: Block Diagram of Series Voltage Controller.

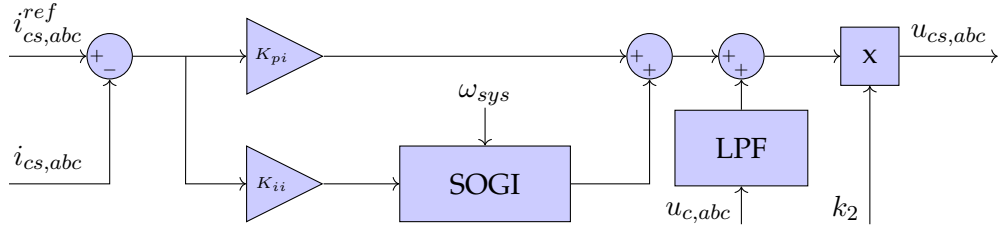


Figure 3.7: Block Diagram of Series Current Controller.

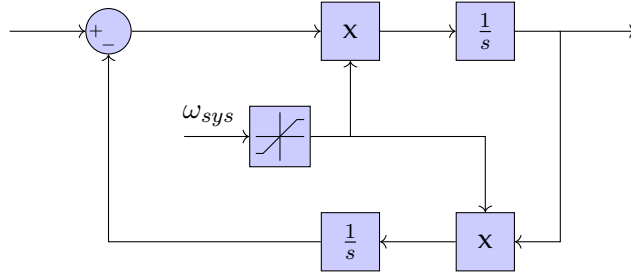


Figure 3.8: Block Diagram of SOGI.

controller that controls each phase individually. The central component of this controller is a second-order generalized integrator (SOGI) shown in Fig. 3.8. The SOGI transfer function provides an infinite gain at the resonant frequency, which allows steady-state error to be canceled when controlling sinusoidal signals at this frequency [46]. This aspect of the SOGI contains many advantages for the studied application, as harmonics should be ignored by the controller. It also allows independent control of each phase, as most other controller structures are less equipped to deal with sinusoidal inputs. Thus, with independent control, the proportional resonant controller provides a simple method to correct unbalanced voltages. In addition to the proportional resonant control, the feedback and feedforward is provided from the measured voltage and current values in the series converter. The feedforward portion is filtered at the system frequency so as to not introduce more harmonics into the output. The control diagrams for the voltage and current controller can be seen in Fig. 3.6 and Fig. 3.7 respectively. The current controller also contains the multiplier for the voltage limit discussed above.

3.4 Shunt Controller

The shunt controller has the goal of regulating the voltage of the DC link. To minimize the sizing of the converter, the converter will normally output zero reactive power. The shunt control is composed of three parts. A power reference generator, a current calculation block, and a current controller. The overview of the shunt controller is shown in Fig. 3.9.

$$\begin{bmatrix} i_{\alpha,cf}^{ref} \\ i_{\beta,cf}^{ref} \end{bmatrix} = \frac{1}{v'_{\alpha,L}^2 + v'_{\beta,L}^2} \begin{bmatrix} u'_{\alpha,L} & u'_{\beta,L} \\ u'_{\beta,L} & -u'_{\alpha,L} \end{bmatrix} \begin{bmatrix} \bar{P}_{ref} \\ \bar{Q}_{ref} \end{bmatrix} \quad (3.6)$$

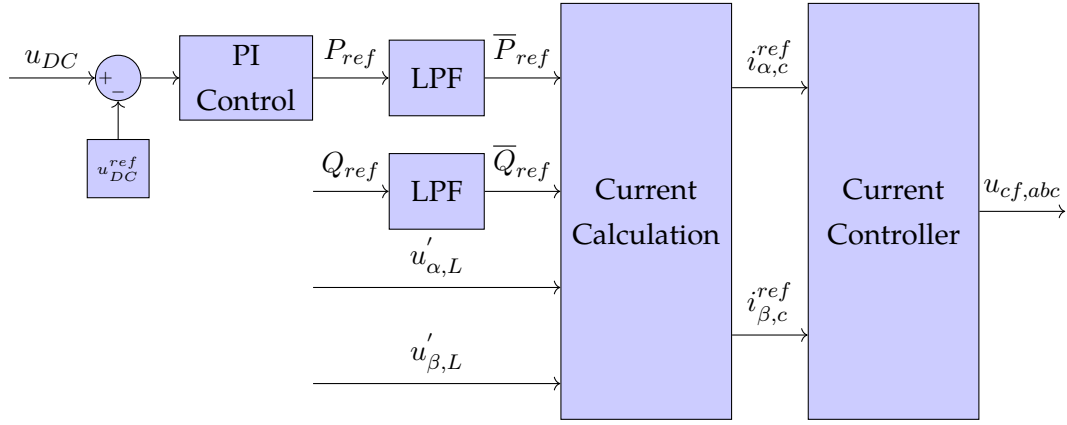


Figure 3.9: Block Diagram of Shunt Controller.

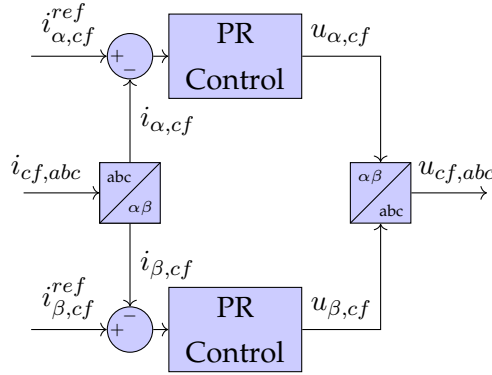


Figure 3.10: Block Diagram of Shunt Current Controller.

The power reference generator uses feedback from the measured DC voltage along with a PI controller to provide a reference for active power. Subsequently, both the active and reactive power references are fed through a low-pass filter to remove any harmonics from the response. These power references and the positive sequence load voltage components from the PSVD are then fed into the current calculation. The current is then obtained according to (3.6). Finally, this current is fed into the PR-based current controller shown in Fig 3.10. It is important to note that this current reference computation is slightly approximated. This occurs because using u_{cf} in the matrix multiplication causes some strong instability since it is the output of the controller. It is assumed that the load voltage is a good approximation since its value will always stay near 1 p.u..

4 Static Model

4.1 Single-Phase

For this first static model, all the voltages are assumed to be balanced. As such, the final representation will be a single-phase model.

4.1.1 Equivalent Circuit

The UPQC circuit found in Fig. 2.8 may be simplified to produce an equivalent circuit representation. Following the assumption that voltages are balanced and additionally assuming the grounds of each converter are connected to the high voltage neutral, the circuit can be modeled as one single phase. Discounting the DC link, the converters can be represented as two independent sources, one voltage source connected in series with the line and one current source connected as a shunt. This equivalent static circuit is shown in Fig. 4.1. As can be seen, the series and shunt filters are included in the model. These filters are LC with a parasitic resistance in the capacitor branch. Due to the high current in the series branch, the voltage drop across the inductor in the LC should be significant without correction by a transformer. Thus, since the filters will weigh in the final design of the transformer, they should be included in the model.

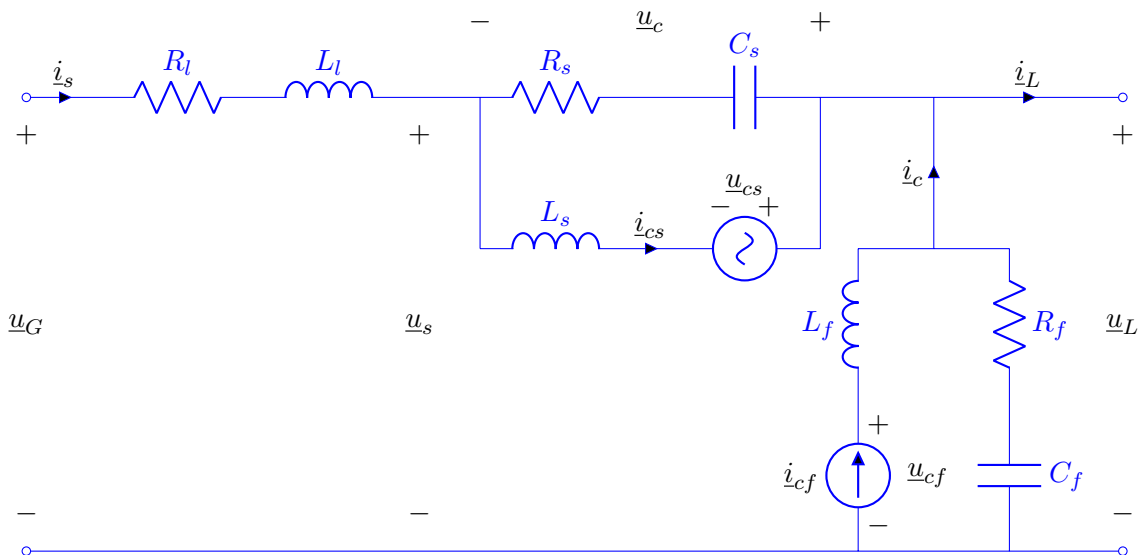


Figure 4.1: UPQC Simplified Model.

However, this circuit representation does not represent the full reality of the circuit. As stated, this representation ignores the DC bus connecting both converters. In addition, the control objectives and the external connections of the circuit are not represented either. As such, some extra assumptions will have to be made to bring this model in line with the dynamic model behavior. These assumptions are the following:

- The load is a PQ load of known active and reactive power.

- The grid voltage is stable and known.
- Load voltage is controlled to have a value of 1.00 p.u. unless the voltage correction limit is reached. If the limit is reached the maximum correction is applied. The difference between the source and load voltage angle is also assumed to be 0. This assumption emulates the control implemented in the series controller
- The converter operates in steady state, as such the active power entering the series converter must equal the active power to ensure the capacitor is neither charging nor discharging. In addition, the reactive power output of the shunt converter is equal to 0. These assumptions emulate the control implemented in the shunt converter.

With the equivalent circuit and these assumptions, the steady-state behaviour of the UPQC has been replicated. With a simple system of equations, the system may now be resolved.

4.1.2 Variables

The first step towards defining the system of equations is to define all of the important variables. These variables can be split into three types: Free variables, dependent variables, and design variables. Both the free and design variables are known beforehand, while the dependent variables will be solved using the system of equations. Sinusoidal quantities will be expressed using complex quantities according to phasor representation. These complex quantities will be described using rectangular coordinates where for any variable \underline{x}_i , $\underline{x}_i = x_{i,\mathbb{R}} + jx_{i,\mathbb{I}}$.

Free Variables

These variables are known through the assumptions made about the equivalent circuit. In reality, these variables will be measured, set by the controllers or portions of the design outside of the scope of the static model.

- Load power (S_L): The load is a PQ load so both complex components (P_s and Q_s) of the load power are known.
- Shunt reactive power (Q_{sh}): The shunt converter is assumed to have 0 reactive power output.
- Grid voltage magnitude ($|\underline{u}_G|$): The grid Thévenin equivalent is assumed to have stable voltage so its magnitude is known.
- Load voltage (\underline{u}_L): The load voltage is assumed to be controlled to have a known magnitude of 1 p.u. In addition, this voltage is assumed to have a zero angle. As such, both the real and imaginary components ($u_{L,\mathbb{R}}$ and $u_{L,\mathbb{I}}$) are known.

- Voltage correction angle ($\angle \underline{u}_{Ls} = \angle \underline{u}_L - \angle \underline{u}_s$): this value is assumed to be 0. Setting this value to 0 is equivalent to assuming $\angle \underline{u}_L = \angle \underline{u}_s = \angle \underline{u}_c$.
- Line impedance (L_l and R_l)
- Series filter values ($L_s^{'}, C_s^{'}, R_s^{'}$)
- Shunt filter values (L_f, C_f, R_f)
- System frequency (ω)

Design Variables

These variables will be used in the optimization of the design.

- Transformer turns ratio (N_T)
- Voltage correction limit ($u_{c,lim}$)

Unknown/Dependent Variables

These are the variables that will be treated as unknowns in the system of equations and will be solved for. They are shown in Table 4.1.

Description	Name	Type	\mathbb{R}	\mathbb{I}	Unknowns
Shunt Current	\underline{i}_c	Complex	$i_{c,\mathbb{R}}$	$i_{c,\mathbb{I}}$	2
Series Converter Current	\underline{i}_{cs}	Complex	$i_{cs,\mathbb{R}}$	$u_{cs,\mathbb{I}}$	2
Shunt Converter Current	\underline{i}_{cf}	Complex	$i_{cf,\mathbb{R}}$	$i_{cf,\mathbb{I}}$	2
Source Current	\underline{i}_s	Complex	$i_{s,\mathbb{R}}$	$i_{s,\mathbb{I}}$	2
Series Correction Voltage	\underline{u}_c	Complex	$u_{c,\mathbb{R}}$	$u_{c,\mathbb{I}}$	2
Series Converter Voltage	\underline{u}_{cs}	Complex	$u_{cs,\mathbb{R}}$	$i_{cs,\mathbb{I}}$	2
Shunt Converter Voltage	\underline{u}_{cf}	Complex	$u_{cf,\mathbb{R}}$	$i_{cf,\mathbb{I}}$	2
Load Current	\underline{i}_L	Complex	$i_{L,\mathbb{R}}$	$i_{L,\mathbb{I}}$	2
Grid Voltage	\underline{u}_G	Complex	$u_{G,\mathbb{R}}$	$u_{G,\mathbb{I}}$	2
Source Voltage	\underline{u}_s	Complex	$u_{s,\mathbb{R}}$	$u_{s,\mathbb{I}}$	2
Total Scalar Unknowns					20

Table 4.1: Single Phase Static Model Unknown Variables.

These variables have values that are specified by the free variables.

4.1.3 Equations

Due to the transformer in the series branch, the base voltage for the series branch will be different based on the transformer turns ratio. As such, the series filter values must be corrected before laying out the system of equations as shown in (4.1)-(4.3).

$$L_s = \frac{L'_s}{N_T^2} \quad (4.1)$$

$$R_s = \frac{R'_s}{N_T^2} \quad (4.2)$$

$$C_s = C'_s N_T^2 \quad (4.3)$$

With the series filter corrected, the system of circuit equations may be laid out. Firstly, the Kirchoff equations of the equivalent circuit are shown. In (4.4)-(4.5), the voltage and current balances at the load connection are shown. In (4.6)-(4.7), the converter currents are obtained with the converter and filter voltage. In (4.8)-(4.9), the current balance of the filters is obtained. In (4.10), the Thévenin equivalent of the grid is shown.

$$\underline{u}_s = \underline{u}_L - \underline{u}_c \quad (4.4)$$

$$\underline{i}_s = \underline{i}_L - \underline{i}_c \quad (4.5)$$

$$\underline{i}_{cs} = \frac{\underline{u}_{cs} - \underline{u}_c}{j\omega L_s} \quad (4.6)$$

$$\underline{i}_{cf} = \frac{\underline{u}_{cf} - \underline{u}_c}{j\omega L_f} \quad (4.7)$$

$$\underline{i}_s = \underline{i}_{cs} - \frac{\underline{u}_c}{R_s + \frac{1}{j\omega C_s}} \quad (4.8)$$

$$\underline{i}_c = \underline{i}_{cf} - \frac{\underline{u}_L}{R_f + \frac{1}{j\omega C_f}} \quad (4.9)$$

$$\underline{i}_s = \frac{\underline{u}_G - \underline{u}_s}{R_l + j\omega L_l} \quad (4.10)$$

Secondly, the equations based on the assumptions about the circuit are shown. In (4.11), the active power balance of the DC bus is shown. In (4.12), the relation for the apparent power of the load is shown. In (4.13), the relation for the reactive power of the shunt converter is shown. In (4.14), the relation for the magnitude of the grid equivalent voltage is shown. In (4.15), the voltage correction angle of the series filter is shown.

$$P_{cs} = -P_{cf} \Rightarrow \Re(\underline{u}_{cs} \cdot \underline{i}_{cs}^*) = \Re(-\underline{u}_{cf} \cdot \underline{i}_{cf}^*) \quad (4.11)$$

$$\underline{S}_L = \underline{u}_L \cdot \underline{i}_L^* \quad (4.12)$$

$$\underline{Q}_{sh} = \mathbb{I} \left(\underline{u}_{cf} \cdot -\underline{i}_{cf}^* \right) \quad (4.13)$$

$$u_{G,mag} = |u_G| \quad (4.14)$$

$$\angle u_c = \angle u_L = 0^\circ \quad (4.15)$$

Separating the real and imaginary portions of the equations, a system of 20 equations is obtained (4.16)-(4.35).

$$u_{s,\mathbb{R}} = u_{L,\mathbb{R}} - u_{c,\mathbb{R}} \quad (4.16)$$

$$u_{s,\mathbb{I}} = u_{L,\mathbb{I}} - u_{c,\mathbb{I}} \quad (4.17)$$

$$i_{s,\mathbb{R}} = i_{L,\mathbb{R}} - i_{c,\mathbb{R}} \quad (4.18)$$

$$i_{s,\mathbb{I}} = i_{L,\mathbb{I}} - i_{c,\mathbb{I}} \quad (4.19)$$

$$i_{cs,\mathbb{R}} = \frac{u_{cs,\mathbb{I}} - u_{c,\mathbb{I}}}{\omega L_s} \quad (4.20)$$

$$i_{cs,\mathbb{I}} = \frac{u_{c,\mathbb{R}} - u_{cs,\mathbb{R}}}{\omega L_s} \quad (4.21)$$

$$i_{cf,\mathbb{R}} = \frac{u_{cf,\mathbb{I}} - u_{L,\mathbb{I}}}{\omega L_f} \quad (4.22)$$

$$i_{cf,\mathbb{I}} = \frac{u_{L,\mathbb{R}} - u_{cf,\mathbb{R}}}{\omega L_s} \quad (4.23)$$

$$i_{s,\mathbb{R}} = i_{cs,\mathbb{R}} - \frac{u_{c,\mathbb{R}} R_s - \frac{u_{c,\mathbb{I}}}{\omega C_s}}{\frac{1}{\omega^2 C_s^2} + R_s^2} \quad (4.24)$$

$$i_{s,\mathbb{I}} = i_{cs,\mathbb{I}} - \frac{u_{c,\mathbb{I}} R_s + \frac{u_{c,\mathbb{R}}}{\omega C_s}}{\frac{1}{\omega^2 C_s^2} + R_s^2} \quad (4.25)$$

$$i_{c,\mathbb{R}} = i_{cf,\mathbb{R}} - \frac{u_{L,\mathbb{R}} R_f - \frac{u_{L,\mathbb{I}}}{\omega C_f}}{\frac{1}{\omega^2 C_f^2} + R_f^2} \quad (4.26)$$

$$i_{c,\mathbb{I}} = i_{cf,\mathbb{R}} - \frac{u_{L,\mathbb{I}} R_f + \frac{u_{L,\mathbb{R}}}{\omega C_f}}{\frac{1}{\omega^2 C_f^2} + R_f^2} \quad (4.27)$$

$$i_{s,\mathbb{R}} = \frac{(u_{G,\mathbb{R}} - u_{s,\mathbb{R}}) R_l + (u_{G,\mathbb{I}} - u_{s,\mathbb{I}}) \omega L_l}{\omega^2 L_l^2 + R_l^2} \quad (4.28)$$

$$i_{s,\mathbb{I}} = \frac{(u_{G,\mathbb{I}} - u_{s,\mathbb{I}}) R_l - (u_{G,\mathbb{R}} - u_{s,\mathbb{R}}) \omega L_l}{\omega^2 L_l^2 + R_l^2} \quad (4.29)$$

$$u_{cs,\mathbb{R}} i_{cs,\mathbb{R}} + u_{cs,\mathbb{I}} i_{cs,\mathbb{I}} = - (u_{cf,\mathbb{R}} i_{cf,\mathbb{R}} + u_{cf,\mathbb{I}} i_{cf,\mathbb{I}}) \quad (4.30)$$

$$P_L = u_{L,\mathbb{R}} \cdot i_{L,\mathbb{R}} + u_{L,\mathbb{I}} \cdot i_{L,\mathbb{I}} \quad (4.31)$$

$$Q_L = u_{L,\mathbb{I}} \cdot i_{L,\mathbb{R}} - u_{L,\mathbb{R}} \cdot i_{L,\mathbb{I}} \quad (4.32)$$

$$Q_{sh} = -(u_{cf,\mathbb{I}} \cdot i_{cf,\mathbb{R}} - u_{cf,\mathbb{R}} \cdot i_{cf,\mathbb{I}}) \quad (4.33)$$

$$\underline{u}_{G,mag}^2 = u_{G,\mathbb{R}}^2 + u_{G,\mathbb{I}}^2 \quad (4.34)$$

$$u_{c,\mathbb{I}} = 0 \quad (4.35)$$

4.1.4 Voltage Limit

The implementation of the voltage limit in the static model involves changing one of the system equations and one of the assumptions about the system. It is triggered in the case $|u_c|$ is found to be larger than $u_{c,lim}$ after running the above system of equations. Once this condition is triggered, $|u_{c,\mathbb{R}}|$ will be set to either $u_{c,lim}$ or $-u_{c,lim}$ based on whether the converter was correcting a sag or swell while $u_{c,\mathbb{I}}$ will retain its value of 0. As such, $|u_L|$ will be treated as unknown, although it will remain at an angle of 0 degrees. Consequently, (4.35) will be replaced with (4.36) in the system of equations.

$$u_{L,\mathbb{I}} = 0 \quad (4.36)$$

4.1.5 Workflow

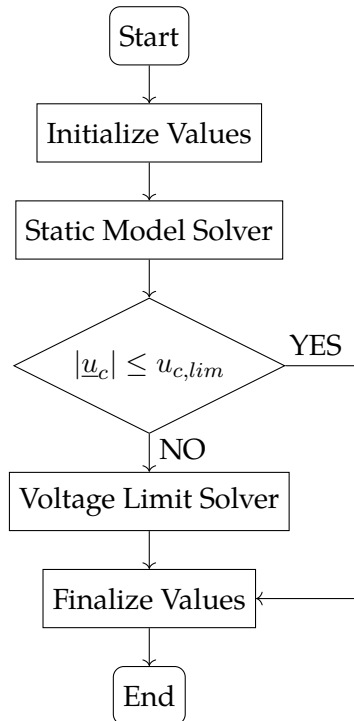


Figure 4.2: Workflow of Single Phase Static Model.

The overall workflow of the single-phase static model will have two possible paths. The condition to determine which path is chosen is based on whether u_c respects the voltage limit condition.

The voltage limit static model will only be run if this condition is not respected. A diagram of the single phase static model workflow is shown in Fig. 4.2.

4.2 Three-Phase

4.2.1 Equivalent Model

The three-phase static model equivalent circuit is given by taking three single-phase equivalent circuits and treating them independently, except for the DC link condition. The power balance of the DC link in this case is shown in (4.38). In order to keep a power balance between the phases, the total power from the series converter will be split evenly between all three phases of the shunt converter as shown in (4.39)-(4.41).

$$P_{cs} = -P_{cf} \quad (4.37)$$

$$\Re(\underline{u}_{cs,a} \cdot \underline{i}_{cs,a}^* + \underline{u}_{cs,b} \cdot \underline{i}_{cs,b}^* + \underline{u}_{cs,c} \cdot \underline{i}_{cs,c}^*) = -\Re(\underline{u}_{cf,a} \cdot \underline{i}_{cf,a}^* + \underline{u}_{cf,b} \cdot \underline{i}_{cf,b}^* + \underline{u}_{cf,c} \cdot \underline{i}_{cf,c}^*) \quad (4.38)$$

$$\Re(\underline{u}_{cs,a} \cdot \underline{i}_{cs,a}^* + \underline{u}_{cs,b} \cdot \underline{i}_{cs,b}^* + \underline{u}_{cs,c} \cdot \underline{i}_{cs,c}^*) = -\frac{1}{3} \Re(\underline{u}_{cf,a} \cdot \underline{i}_{cf,a}^*) \quad (4.39)$$

$$\Re(\underline{u}_{cs,a} \cdot \underline{i}_{cs,a}^* + \underline{u}_{cs,b} \cdot \underline{i}_{cs,b}^* + \underline{u}_{cs,c} \cdot \underline{i}_{cs,c}^*) = -\frac{1}{3} \Re(\underline{u}_{cf,b} \cdot \underline{i}_{cf,b}^*) \quad (4.40)$$

$$\Re(\underline{u}_{cs,a} \cdot \underline{i}_{cs,a}^* + \underline{u}_{cs,b} \cdot \underline{i}_{cs,b}^* + \underline{u}_{cs,c} \cdot \underline{i}_{cs,c}^*) = -\frac{1}{3} \Re(\underline{u}_{cf,c} \cdot \underline{i}_{cf,c}^*) \quad (4.41)$$

4.2.2 Variables

Description	Name	Type	\mathbb{R}	\mathbb{I}	Unknowns
Shunt Current	\underline{i}_c	Complex	$i_{c,\mathbb{R}}$	$i_{c,\mathbb{I}}$	6
Series Converter Current	\underline{i}_{cs}	Complex	$i_{cs,\mathbb{R}}$	$u_{cs,\mathbb{I}}$	6
Shunt Converter Current	\underline{i}_{cf}	Complex	$i_{cf,\mathbb{R}}$	$i_{cf,\mathbb{I}}$	6
Source Current	\underline{i}_s	Complex	$i_{s,\mathbb{R}}$	$i_{s,\mathbb{I}}$	6
Series Correction Voltage	\underline{u}_c	Complex	$u_{c,\mathbb{R}}$	$u_{c,\mathbb{I}}$	6
Series Converter Voltage	\underline{u}_{cs}	Complex	$u_{cs,\mathbb{R}}$	$i_{cs,\mathbb{I}}$	6
Shunt Converter Voltage	\underline{u}_{cf}	Complex	$u_{cf,\mathbb{R}}$	$i_{cf,\mathbb{I}}$	6
Load Current	\underline{i}_L	Complex	$i_{L,\mathbb{R}}$	$i_{L,\mathbb{I}}$	6
Grid Voltage	\underline{u}_G	Complex	$u_{G,\mathbb{R}}$	$u_{G,\mathbb{I}}$	6
Source Voltage	\underline{u}_s	Complex	$u_{s,\mathbb{R}}$	$u_{s,\mathbb{I}}$	6
Total Scalar Unknowns				60	

Table 4.2: Three Phase Static Model Unknown Variables.

The assumptions made about the circuit and unknowns of the circuit are also the same as in the single-phase case. However, since there is an unknown variable for each phase, the total number of unknowns is 60 instead of 20. These are outlined in Tab. 4.2.

4.2.3 Equations

As the equivalent circuits are treated independently outside of the DC link, the equations can be duplicated for each independent phase. As such, there is a system of 60 equations for 60 unknowns. These are shown below in (4.42)-(4.101).

$$\underline{u}_{s,a \mathbb{R}} = \underline{u}_{L,a \mathbb{R}} - \underline{u}_{c,a \mathbb{R}} \quad (4.42)$$

$$\underline{u}_{s,a \mathbb{I}} = \underline{u}_{L,a \mathbb{I}} - \underline{u}_{c,a \mathbb{I}} \quad (4.43)$$

$$\underline{u}_{s,b \mathbb{R}} = \underline{u}_{L,b \mathbb{R}} - \underline{u}_{c,b \mathbb{R}} \quad (4.44)$$

$$\underline{u}_{s,b \mathbb{I}} = \underline{u}_{L,b \mathbb{I}} - \underline{u}_{c,b \mathbb{I}} \quad (4.45)$$

$$\underline{u}_{s,c \mathbb{R}} = \underline{u}_{L,c \mathbb{R}} - \underline{u}_{c,c \mathbb{R}} \quad (4.46)$$

$$\underline{u}_{s,c \mathbb{I}} = \underline{u}_{L,c \mathbb{I}} - \underline{u}_{c,c \mathbb{I}} \quad (4.47)$$

$$\underline{i}_{s,a \mathbb{R}} = \underline{i}_{L,a \mathbb{R}} - \underline{i}_{c,a \mathbb{R}} \quad (4.48)$$

$$\underline{i}_{s,a \mathbb{I}} = \underline{i}_{L,a \mathbb{I}} - \underline{i}_{c,a \mathbb{I}} \quad (4.49)$$

$$\underline{i}_{s,b \mathbb{R}} = \underline{i}_{L,b \mathbb{R}} - \underline{i}_{c,b \mathbb{R}} \quad (4.50)$$

$$\underline{i}_{s,b \mathbb{I}} = \underline{i}_{L,b \mathbb{I}} - \underline{i}_{c,b \mathbb{I}} \quad (4.51)$$

$$\underline{i}_{s,c \mathbb{R}} = \underline{i}_{L,c \mathbb{R}} - \underline{i}_{c,c \mathbb{R}} \quad (4.52)$$

$$\underline{i}_{s,c \mathbb{I}} = \underline{i}_{L,c \mathbb{I}} - \underline{i}_{c,c \mathbb{I}} \quad (4.53)$$

$$\underline{i}_{cs,a \mathbb{R}} = \frac{\underline{u}_{cs,a \mathbb{I}} - \underline{u}_{c,a \mathbb{I}}}{\omega L_s} \quad (4.54)$$

$$\underline{i}_{cs,a \mathbb{I}} = \frac{\underline{u}_{c,a \mathbb{R}} - \underline{u}_{cs,a \mathbb{R}}}{\omega L_s} \quad (4.55)$$

$$\underline{i}_{cs,b \mathbb{R}} = \frac{\underline{u}_{cs,b \mathbb{I}} - \underline{u}_{c,b \mathbb{I}}}{\omega L_s} \quad (4.56)$$

$$\underline{i}_{cs,b \mathbb{I}} = \frac{\underline{u}_{c,b \mathbb{R}} - \underline{u}_{cs,b \mathbb{R}}}{\omega L_s} \quad (4.57)$$

$$\underline{i}_{cs,c \mathbb{R}} = \frac{\underline{u}_{cs,c \mathbb{I}} - \underline{u}_{c,c \mathbb{I}}}{\omega L_s} \quad (4.58)$$

$$\underline{i}_{cs,c \mathbb{I}} = \frac{\underline{u}_{c,c \mathbb{R}} - \underline{u}_{cs,c \mathbb{R}}}{\omega L_s} \quad (4.59)$$

$$\underline{i}_{cf,a \mathbb{R}} = \frac{\underline{u}_{cf,a \mathbb{I}} - \underline{u}_{L,a \mathbb{I}}}{\omega L_f} \quad (4.60)$$

$$\underline{i}_{cf,a \mathbb{I}} = \frac{\underline{u}_{L,a \mathbb{R}} - \underline{u}_{cf,a \mathbb{R}}}{\omega L_f} \quad (4.61)$$

$$\underline{i}_{cf,b \mathbb{R}} = \frac{\underline{u}_{cf,b \mathbb{I}} - \underline{u}_{L,b \mathbb{I}}}{\omega L_f} \quad (4.62)$$

$$\underline{i}_{cf,b\mathbb{I}} = \frac{\underline{u}_{L,b\mathbb{R}} - \underline{u}_{cf,b\mathbb{R}}}{\omega L_f} \quad (4.63)$$

$$\underline{i}_{cf,c\mathbb{R}} = \frac{\underline{u}_{cf,c\mathbb{I}} - \underline{u}_{L,c\mathbb{I}}}{\omega L_f} \quad (4.64)$$

$$\underline{i}_{cf,c\mathbb{I}} = \frac{\underline{u}_{cf,c\mathbb{R}} - \underline{u}_{L,c\mathbb{R}}}{\omega L_f} \quad (4.65)$$

$$i_{s,a\mathbb{R}} = i_{cs,a\mathbb{R}} - \frac{\underline{u}_{c,a\mathbb{R}} R_s - \frac{\underline{u}_{c,a\mathbb{I}}}{\omega C_s}}{\frac{1}{\omega^2 C_s^2} + R_s^2} \quad (4.66)$$

$$i_{s,a\mathbb{I}} = i_{cs,a\mathbb{I}} - \frac{\underline{u}_{c,a\mathbb{I}} R_s + \frac{\underline{u}_{c,a\mathbb{R}}}{\omega C_s}}{\frac{1}{\omega^2 C_s^2} + R_s^2} \quad (4.67)$$

$$i_{s,b\mathbb{R}} = i_{cs,b\mathbb{R}} - \frac{\underline{u}_{c,b\mathbb{R}} R_s - \frac{\underline{u}_{c,b\mathbb{I}}}{\omega C_s}}{\frac{1}{\omega^2 C_s^2} + R_s^2} \quad (4.68)$$

$$i_{s,b\mathbb{I}} = i_{cs,b\mathbb{I}} - \frac{\underline{u}_{c,b\mathbb{I}} R_s + \frac{\underline{u}_{c,b\mathbb{R}}}{\omega C_s}}{\frac{1}{\omega^2 C_s^2} + R_s^2} \quad (4.69)$$

$$i_{s,c\mathbb{R}} = i_{cs,c\mathbb{R}} - \frac{\underline{u}_{c,c\mathbb{R}} R_s - \frac{\underline{u}_{c,c\mathbb{I}}}{\omega C_s}}{\frac{1}{\omega^2 C_s^2} + R_s^2} \quad (4.70)$$

$$i_{s,c\mathbb{I}} = i_{cs,c\mathbb{I}} - \frac{\underline{u}_{c,c\mathbb{I}} R_s + \frac{\underline{u}_{c,c\mathbb{R}}}{\omega C_s}}{\frac{1}{\omega^2 C_s^2} + R_s^2} \quad (4.71)$$

$$i_{c,a\mathbb{R}} = i_{cf,a\mathbb{R}} - \frac{\underline{u}_{L,a\mathbb{R}} R_f - \frac{\underline{u}_{L,a\mathbb{I}}}{\omega C_f}}{\frac{1}{\omega^2 C_f^2} + R_f^2} \quad (4.72)$$

$$i_{c,a\mathbb{I}} = i_{cf,a\mathbb{I}} - \frac{\underline{u}_{L,a\mathbb{I}} R_f + \frac{\underline{u}_{L,a\mathbb{R}}}{\omega C_f}}{\frac{1}{\omega^2 C_f^2} + R_f^2} \quad (4.73)$$

$$i_{c,b\mathbb{R}} = i_{cf,b\mathbb{R}} - \frac{\underline{u}_{L,b\mathbb{R}} R_f - \frac{\underline{u}_{L,b\mathbb{I}}}{\omega C_f}}{\frac{1}{\omega^2 C_f^2} + R_f^2} \quad (4.74)$$

$$i_{c,b\mathbb{I}} = i_{cf,b\mathbb{I}} - \frac{\underline{u}_{L,b\mathbb{I}} R_f + \frac{\underline{u}_{L,b\mathbb{R}}}{\omega C_f}}{\frac{1}{\omega^2 C_f^2} + R_f^2} \quad (4.75)$$

$$i_{c,c\mathbb{R}} = i_{cf,c\mathbb{R}} - \frac{\underline{u}_{L,c\mathbb{R}} R_f - \frac{\underline{u}_{L,c\mathbb{I}}}{\omega C_f}}{\frac{1}{\omega^2 C_f^2} + R_f^2} \quad (4.76)$$

$$i_{c,c\mathbb{I}} = i_{cf,c\mathbb{I}} - \frac{\underline{u}_{L,c\mathbb{I}} R_f + \frac{\underline{u}_{L,c\mathbb{R}}}{\omega C_f}}{\frac{1}{\omega^2 C_f^2} + R_f^2} \quad (4.77)$$

$$i_{s,a\mathbb{R}} = \frac{(u_{G,a\mathbb{R}} - u_{s,a\mathbb{R}}) R_l - (u_{G,a\mathbb{I}} - u_{s,a\mathbb{I}}) \omega L_l}{\omega^2 L_l^2 + R_l^2} \quad (4.78)$$

$$i_{s,a\mathbb{I}} = \frac{(u_{G,a\mathbb{I}} - u_{s,a\mathbb{I}}) R_l + (u_{G,a\mathbb{R}} - u_{s,a\mathbb{R}}) \omega L_l}{\omega^2 L_l^2 + R_l^2} \quad (4.79)$$

$$i_{s,b\mathbb{R}} = \frac{(u_{G,b\mathbb{R}} - u_{s,b\mathbb{R}}) R_l - (u_{G,b\mathbb{I}} - u_{s,b\mathbb{I}}) \omega L_l}{\omega^2 L_l^2 + R_l^2} \quad (4.80)$$

$$i_{s,b\mathbb{I}} = \frac{(u_{G,b\mathbb{I}} - u_{s,b\mathbb{I}}) R_l + (u_{G,b\mathbb{R}} - u_{s,b\mathbb{R}}) \omega L_l}{\omega^2 L_l^2 + R_l^2} \quad (4.81)$$

$$i_{s,c\mathbb{R}} = \frac{(u_{G,c\mathbb{R}} - u_{s,c\mathbb{R}}) R_l - (u_{G,c\mathbb{I}} - u_{s,c\mathbb{I}}) \omega L_l}{\omega^2 L_l^2 + R_l^2} \quad (4.82)$$

$$i_{s,c\mathbb{I}} = \frac{(u_{G,c\mathbb{I}} - u_{s,c\mathbb{I}}) R_l + (u_{G,c\mathbb{R}} - u_{s,c\mathbb{R}}) \omega L_l}{\omega^2 L_l^2 + R_l^2} \quad (4.83)$$

$$\begin{aligned} & u_{cs,a\mathbb{R}} \cdot i_{cs,a\mathbb{R}} + u_{cs,a\mathbb{I}} \cdot i_{cs,a\mathbb{I}} + u_{cs,b\mathbb{R}} \cdot i_{cs,b\mathbb{R}} + u_{cs,b\mathbb{I}} \cdot i_{cs,b\mathbb{I}} \\ & + u_{cs,c\mathbb{R}} \cdot i_{cs,c\mathbb{R}} + u_{cs,c\mathbb{I}} \cdot i_{cs,c\mathbb{I}} = -\frac{1}{3} (u_{cf,a\mathbb{R}} \cdot i_{cf,a\mathbb{R}} + u_{cf,a\mathbb{I}} \cdot i_{cf,a\mathbb{I}}) \end{aligned} \quad (4.84)$$

$$\begin{aligned} & u_{cs,a\mathbb{R}} \cdot i_{cs,a\mathbb{R}} + u_{cs,a\mathbb{I}} \cdot i_{cs,a\mathbb{I}} + u_{cs,b\mathbb{R}} \cdot i_{cs,b\mathbb{R}} + u_{cs,b\mathbb{I}} \cdot i_{cs,b\mathbb{I}} \\ & + u_{cs,c\mathbb{R}} \cdot i_{cs,c\mathbb{R}} + u_{cs,c\mathbb{I}} \cdot i_{cs,c\mathbb{I}} = -\frac{1}{3} (u_{cf,b\mathbb{R}} \cdot i_{cf,b\mathbb{R}} + u_{cf,b\mathbb{I}} \cdot i_{cf,b\mathbb{I}}) \end{aligned} \quad (4.85)$$

$$\begin{aligned} & u_{cs,a\mathbb{R}} \cdot i_{cs,a\mathbb{R}} + u_{cs,a\mathbb{I}} \cdot i_{cs,a\mathbb{I}} + u_{cs,b\mathbb{R}} \cdot i_{cs,b\mathbb{R}} + u_{cs,b\mathbb{I}} \cdot i_{cs,b\mathbb{I}} \\ & + u_{cs,c\mathbb{R}} \cdot i_{cs,c\mathbb{R}} + u_{cs,c\mathbb{I}} \cdot i_{cs,c\mathbb{I}} = -\frac{1}{3} (u_{cf,c\mathbb{R}} \cdot i_{cf,c\mathbb{R}} + u_{cf,c\mathbb{I}} \cdot i_{cf,c\mathbb{I}}) \end{aligned} \quad (4.86)$$

$$P_{L,a} = u_{L,a\mathbb{R}} \cdot i_{L,a\mathbb{R}} + u_{L,a\mathbb{I}} \cdot i_{L,a\mathbb{I}} \quad (4.87)$$

$$P_{L,b} = u_{L,b\mathbb{R}} \cdot i_{L,b\mathbb{R}} + u_{L,b\mathbb{I}} \cdot i_{L,b\mathbb{I}} \quad (4.88)$$

$$P_{L,c} = u_{L,c\mathbb{R}} \cdot i_{L,c\mathbb{R}} + u_{L,c\mathbb{I}} \cdot i_{L,c\mathbb{I}} \quad (4.89)$$

$$Q_{L,a} = u_{L,a\mathbb{I}} \cdot i_{L,a\mathbb{R}} - u_{L,a\mathbb{R}} \cdot i_{L,a\mathbb{I}} \quad (4.90)$$

$$Q_{L,b} = u_{L,b\mathbb{I}} \cdot i_{L,b\mathbb{R}} - u_{L,b\mathbb{R}} \cdot i_{L,b\mathbb{I}} \quad (4.91)$$

$$Q_{L,c} = u_{L,c\mathbb{I}} \cdot i_{L,c\mathbb{R}} - u_{L,c\mathbb{R}} \cdot i_{L,c\mathbb{I}} \quad (4.92)$$

$$Q_{sh,a} = -(u_{cf,a\mathbb{I}} \cdot i_{cf,a\mathbb{R}} - u_{cf,a\mathbb{R}} \cdot i_{cf,a\mathbb{I}}) \quad (4.93)$$

$$Q_{sh,b} = -(u_{cf,b\mathbb{I}} \cdot i_{cf,b\mathbb{R}} - u_{cf,b\mathbb{R}} \cdot i_{cf,b\mathbb{I}}) \quad (4.94)$$

$$Q_{sh,c} = -(u_{cf,c\mathbb{I}} \cdot i_{cf,c\mathbb{R}} - u_{cf,c\mathbb{R}} \cdot i_{cf,c\mathbb{I}}) \quad (4.95)$$

$$\underline{u}_{G,a mag}^2 = u_{G,a\mathbb{R}}^2 + u_{G,a\mathbb{I}}^2 \quad (4.96)$$

$$\underline{u}_{G,b mag}^2 = u_{G,b\mathbb{R}}^2 + u_{G,b\mathbb{I}}^2 \quad (4.97)$$

$$\underline{u}_{G,c mag}^2 = u_{G,c\mathbb{R}}^2 + u_{G,c\mathbb{I}}^2 \quad (4.98)$$

$$u_{c,a\mathbb{I}} = 0 \quad (4.99)$$

$$\sin\left(\frac{2\pi}{3}\right) \cdot u_{c,b\mathbb{I}} + \cos\left(\frac{2\pi}{3}\right) \cdot u_{c,b\mathbb{I}} = 0 \quad (4.100)$$

$$\sin\left(-\frac{2\pi}{3}\right) \cdot u_{c,c\mathbb{I}} + \cos\left(-\frac{2\pi}{3}\right) \cdot u_{c,c\mathbb{I}} = 0 \quad (4.101)$$

5 Validation

Now that both models have been completed, verifying that they display the correct behavior is important. For the dynamic model, it will be checked whether the control has managed to achieve the control objectives. For the static model, its behavior will be compared to the steady state behavior of the dynamic model to verify both models are close enough that the static model may be used when sizing the components.

5.1 Dynamic

For the dynamic model, a sweep of grid voltages between 1.1 and 0.9 p.u. is completed for loads at three different power factors. From these simulations, seven different measurements are investigated to verify whether the control achieves its objectives. These seven measurements are the load and source voltage, the series and shunt active and reactive powers, and the DC link voltage. They are investigated both with and without the voltage limit applied.

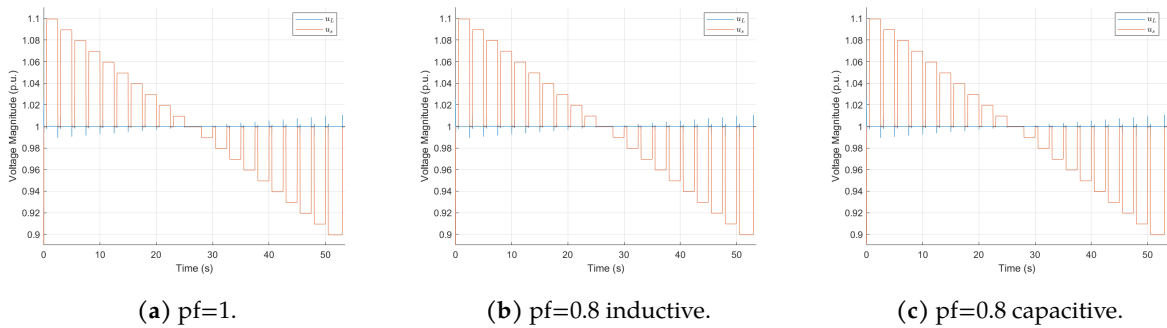


Figure 5.1: Load and Source Voltage Magnitude with Sweep of Grid Voltages from 1.1 to 0.9 p.u..

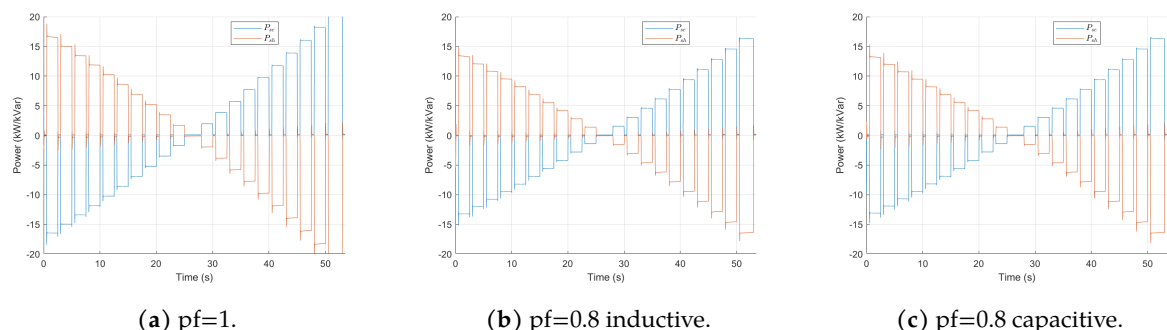


Figure 5.2: Series and Shunt Converter Active Power with Sweep of Grid Voltages from 1.1 to 0.9 p.u..

Firstly, the load and source voltage are shown in Figs. 5.1&5.5. The goal of these graphs is to verify the load voltage is kept at 1 p.u. unless the voltage correction exceeds the voltage limit. As can be seen, while the source voltages are varied up and down due to the sweep of grid voltages, the load voltage remains stable at 1 p.u. for all the grid voltages in the case without the voltage limit. When the voltage limit is added, the load voltage increases or decreases with the same

slope as the source voltage as soon as the voltage limit is reached. This behaviour is in line with what is expected from the series converter.

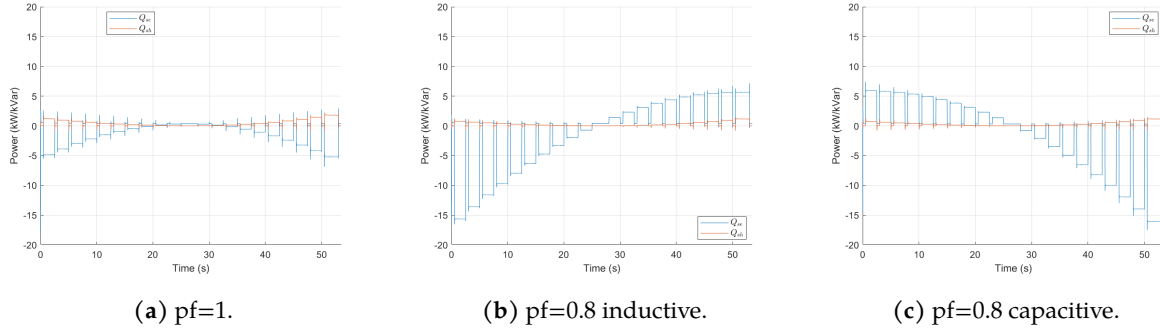


Figure 5.3: Series and Shunt Converter Reactive Power with Sweep of Grid Voltages from 1.1 to 0.9 p.u..

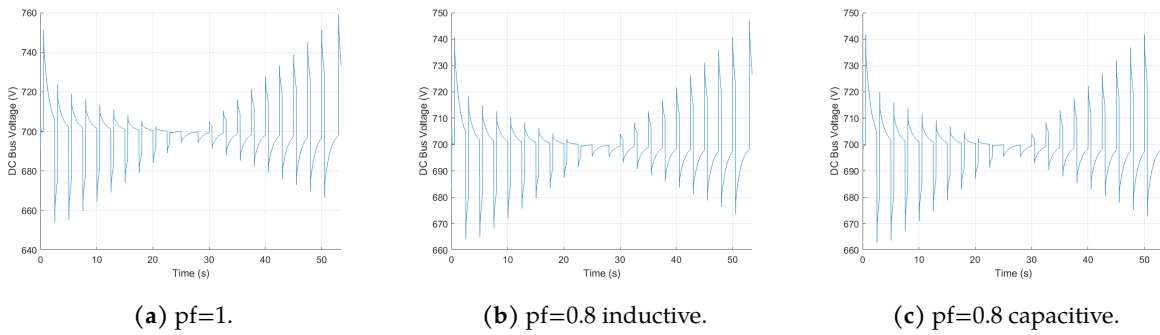


Figure 5.4: DC Voltage with Sweep of Grid Voltages from 1.1 to 0.9 p.u..

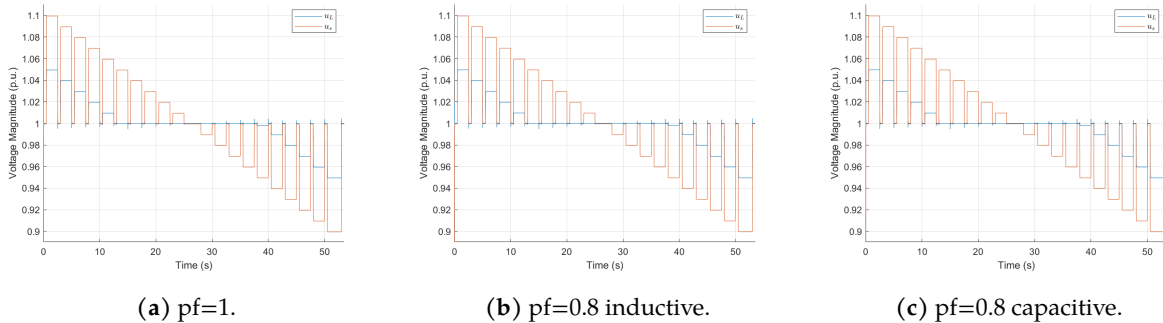


Figure 5.5: Load and Source Voltage Magnitude with Sweep of Grid Voltages from 1.1 to 0.9 p.u. and Voltage Correction Limit of 20 V.

Secondly, the active power of the series and shunt converter is shown in Figs. 5.2&5.6. The goal of these graphs is to verify that the active power flow at steady state is equal for the series and shunt converters to ensure the DC link is not charging or discharging any more than expected. This behavior can indeed be observed in both the graphs. In addition, with the voltage limit implemented, the active power levels off for both converters, which would be expected as well.

Thirdly, the reactive power of the series and shunt converter is shown in Figs. 5.3&5.7. The goal

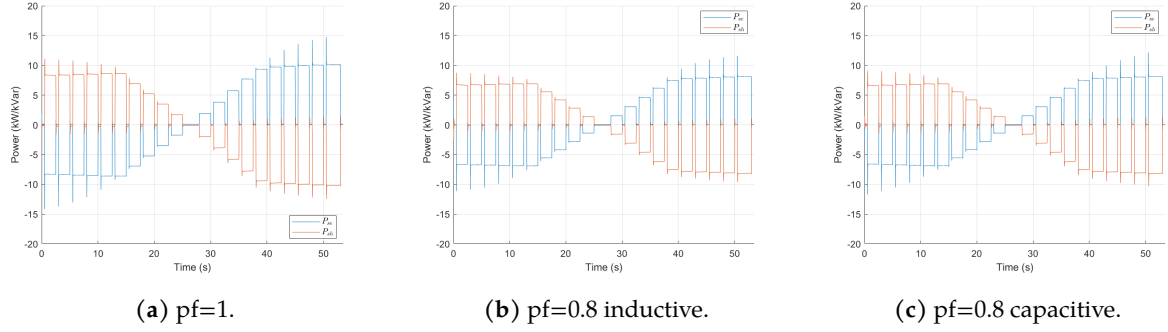


Figure 5.6: Series and Shunt Converter Active Power with Sweep of Grid Voltages from 1.1 to 0.9 p.u. and Voltage Correction Limit of 20 V.

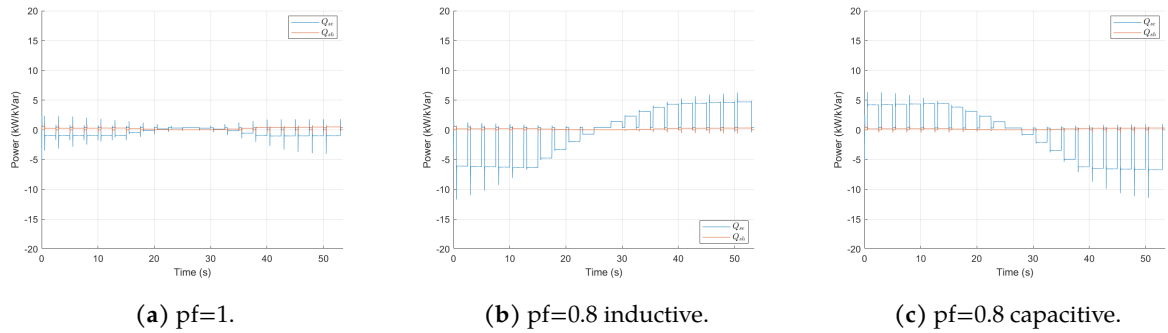


Figure 5.7: Series and Shunt Converter Reactive Power with Sweep of Grid Voltages from 1.1 to 0.9 p.u. and Voltage Correction Limit of 20 V.

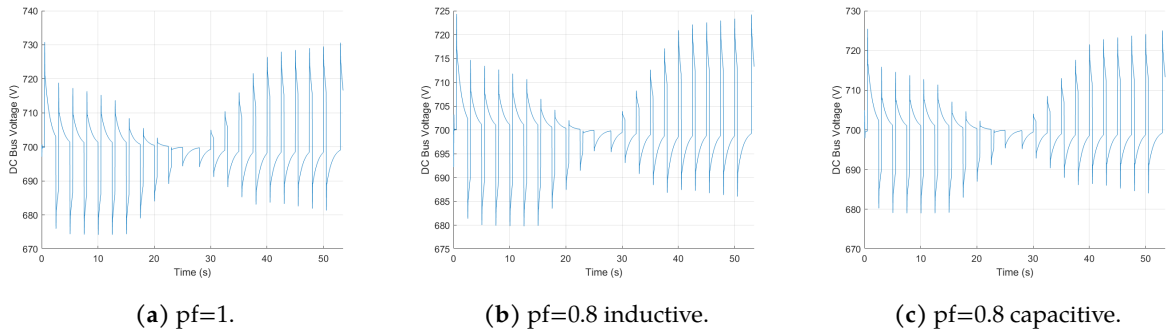


Figure 5.8: DC Voltage with Sweep of Grid Voltages from 1.1 to 0.9 p.u. and Voltage Correction Limit of 20 V.

of these graphs is to check whether the condition of zero reactive power output from the shunt converter is respected. When looking at the graph, a slight discrepancy can be observed. At the 0.9 and 1.1 p.u. data points, the reactive power is close to 1 kvar. This discrepancy can be explained by the approximation made in the current calculation in (3.6), where the load voltage was used instead of the converter voltage. Since this has minimal effect on the total converter power (approximately .03 kVA) and the reactive power seems to grow proportionally with the

active power, this error will be deemed acceptable.

Finally, the voltage of the DC link capacitor is shown in Figs. 5.4&5.8. This graph is to verify the sizing of the DC link capacitor. In the range of power outputs studied, the voltage should not vary more than 5% from the nominal DC voltage. Since the voltage correction in the AC system will likely not be corrected more than 0.05 p.u., the maximum expected variation in the DC link voltage will be around 25V, under 5% of the nominal DC voltage of 700V.

5.2 Static

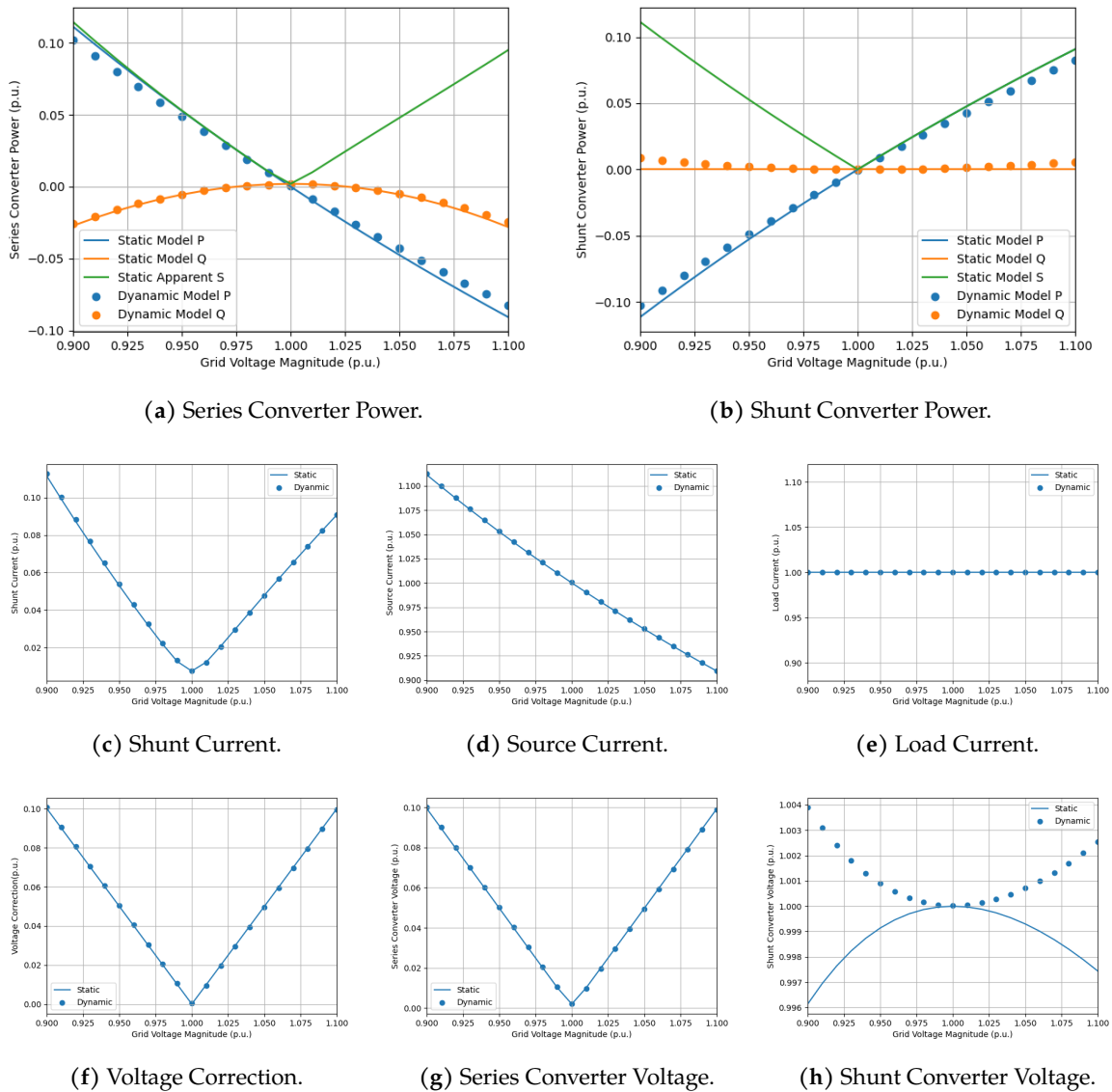


Figure 5.9: Static Model Validation with a Load Power Factor $\text{pf}=1$ and Transformer Ratio of $N_T=20$.

In the static validation, eight different graphs are reviewed in each scenario to make sure the static and dynamic models show similar results. Of these eight, five show little to no deviation

for all scenarios. These are the shunt current, source current, load current, voltage correction, and series converter voltage graphs. Two of them show small deviations. Indeed, the active power of both the series and shunt converter is a small overestimation of the one provided in the dynamic model. Although the error is never more than 1% in the worst case seen in Fig. 5.16a. This can be explained using two explanations. The first is the slight deviation of the dynamic model from the ideal behavior, which could affect the current angle of the source current. The second is the omission of the series transformer parameters from the equivalent model. While the parameters were set to near ideal in the dynamic model, the specifics of the Simulink block are still unknown. The final graph which shows the shunt converter voltage is the one that shows the largest deviation in behavior, although the maximum error is around 0.8% as seen in Fig. 5.10h.

As such, the static model is shown to be validated with the dynamic model, albeit with a small error that could be rectified by adding more elements to the equivalent circuit.

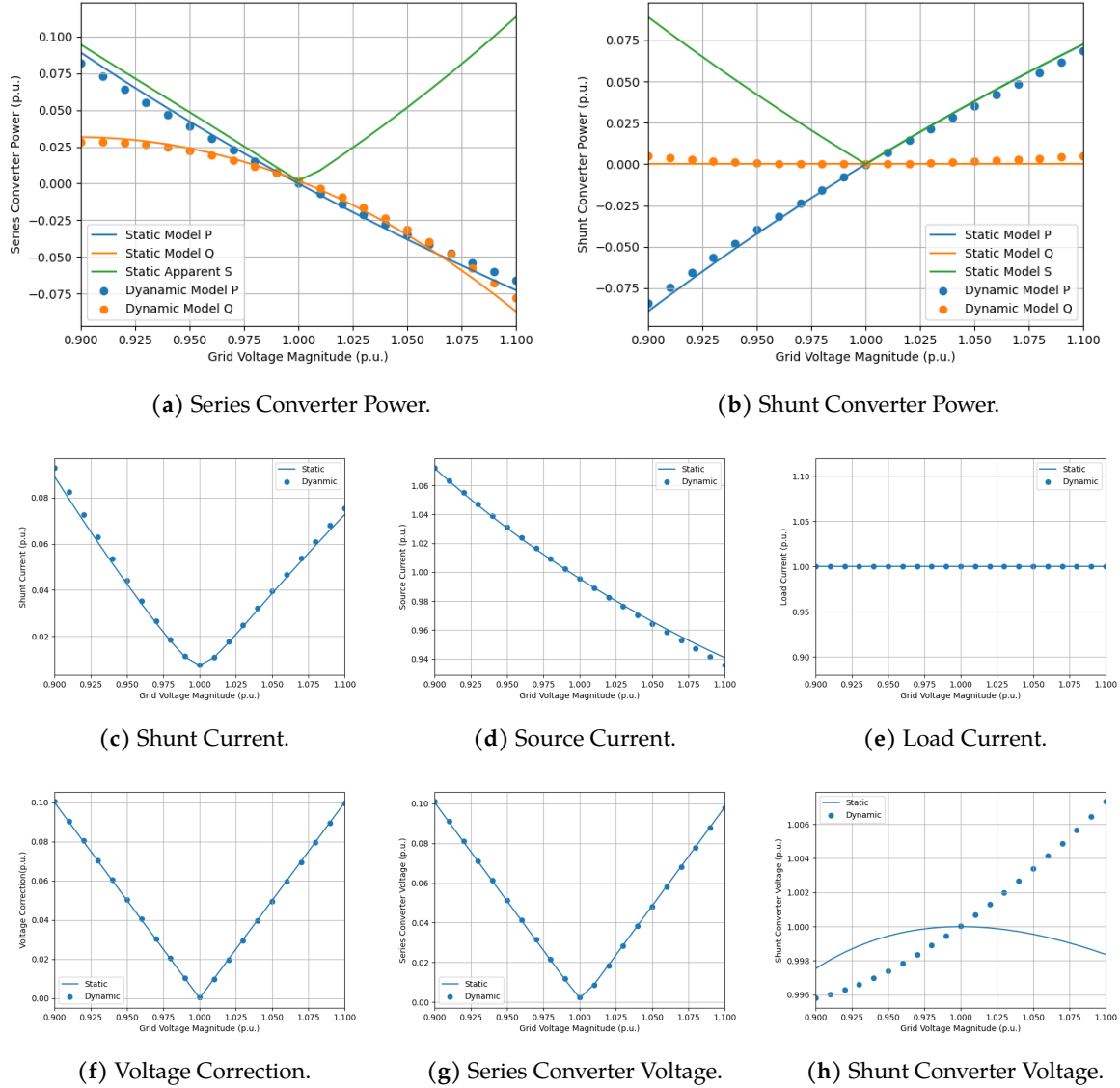


Figure 5.10: Static Model Validation with an Inductive Load Power Factor $\text{pf}=0.8$ and Transformer Ratio of $N_T=20$.

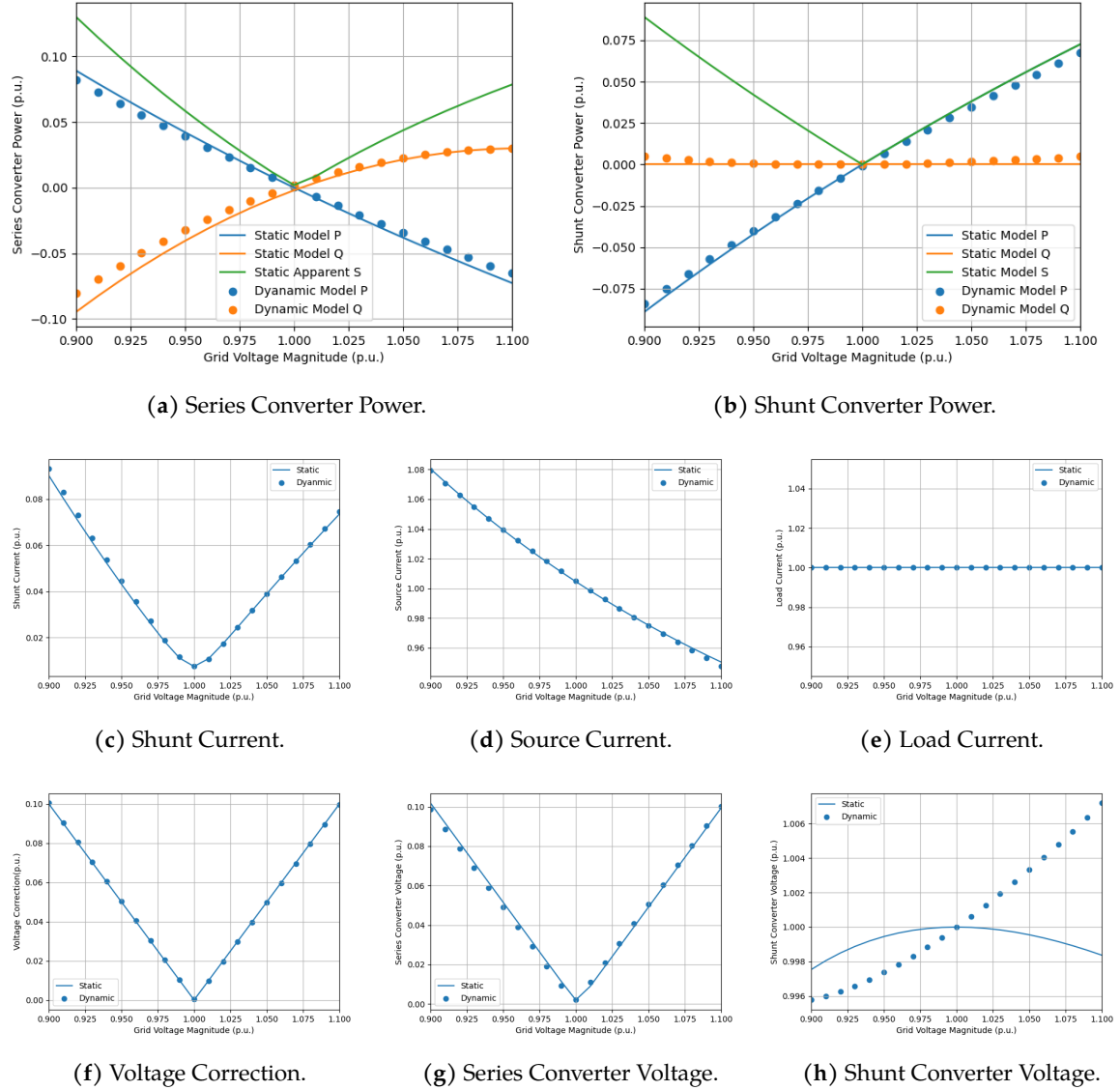


Figure 5.11: Static Model Validation with an Capacitive Load Power Factor $\text{pf}=0.8$ and Transformer Ratio of $N_T=20$.

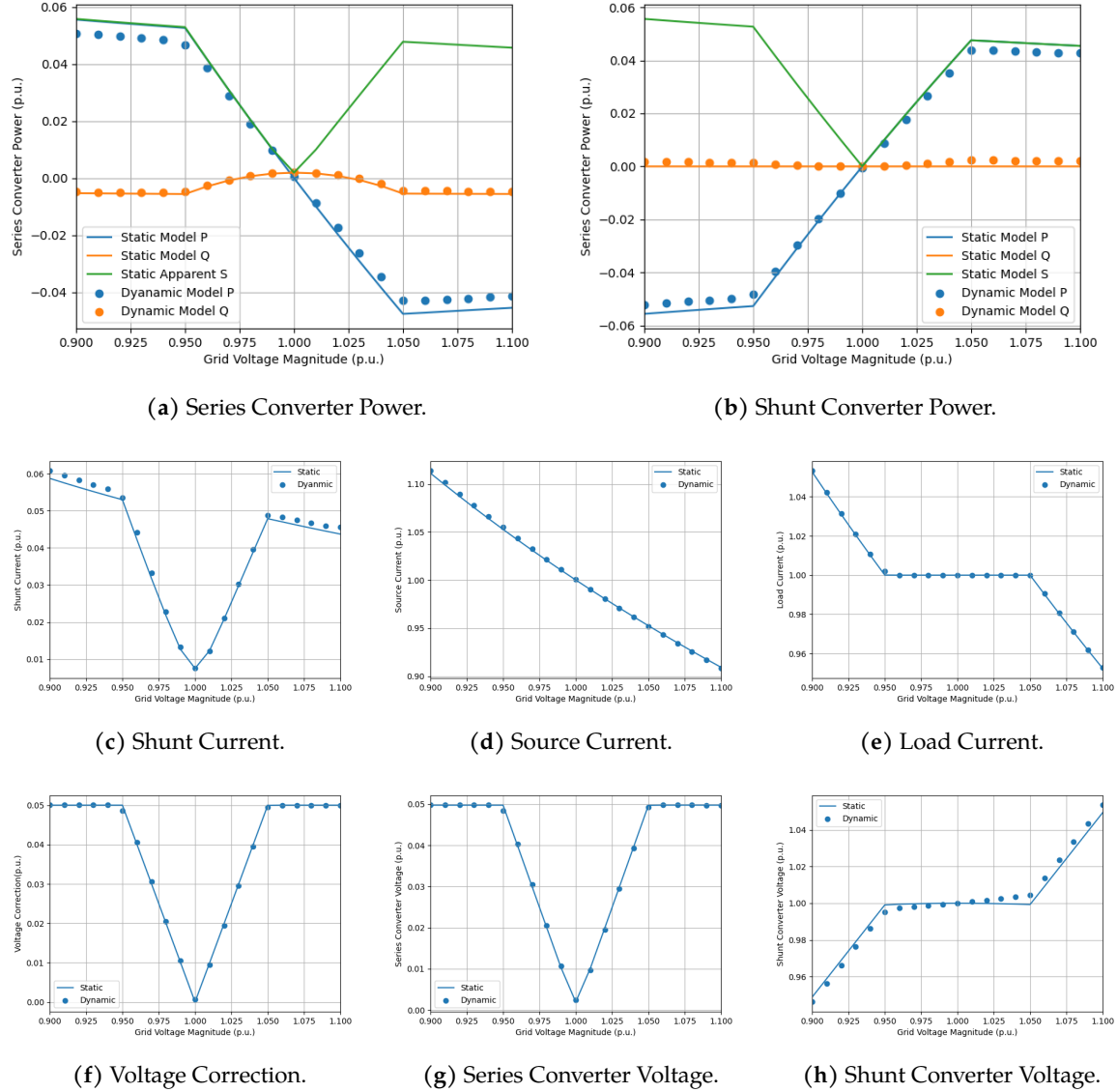


Figure 5.12: Static Model Validation with a Voltage Limit of 0.05 p.u., a Load Power Factor $\text{pf}=1$ and Transformer Ratio of $N_T=20$.

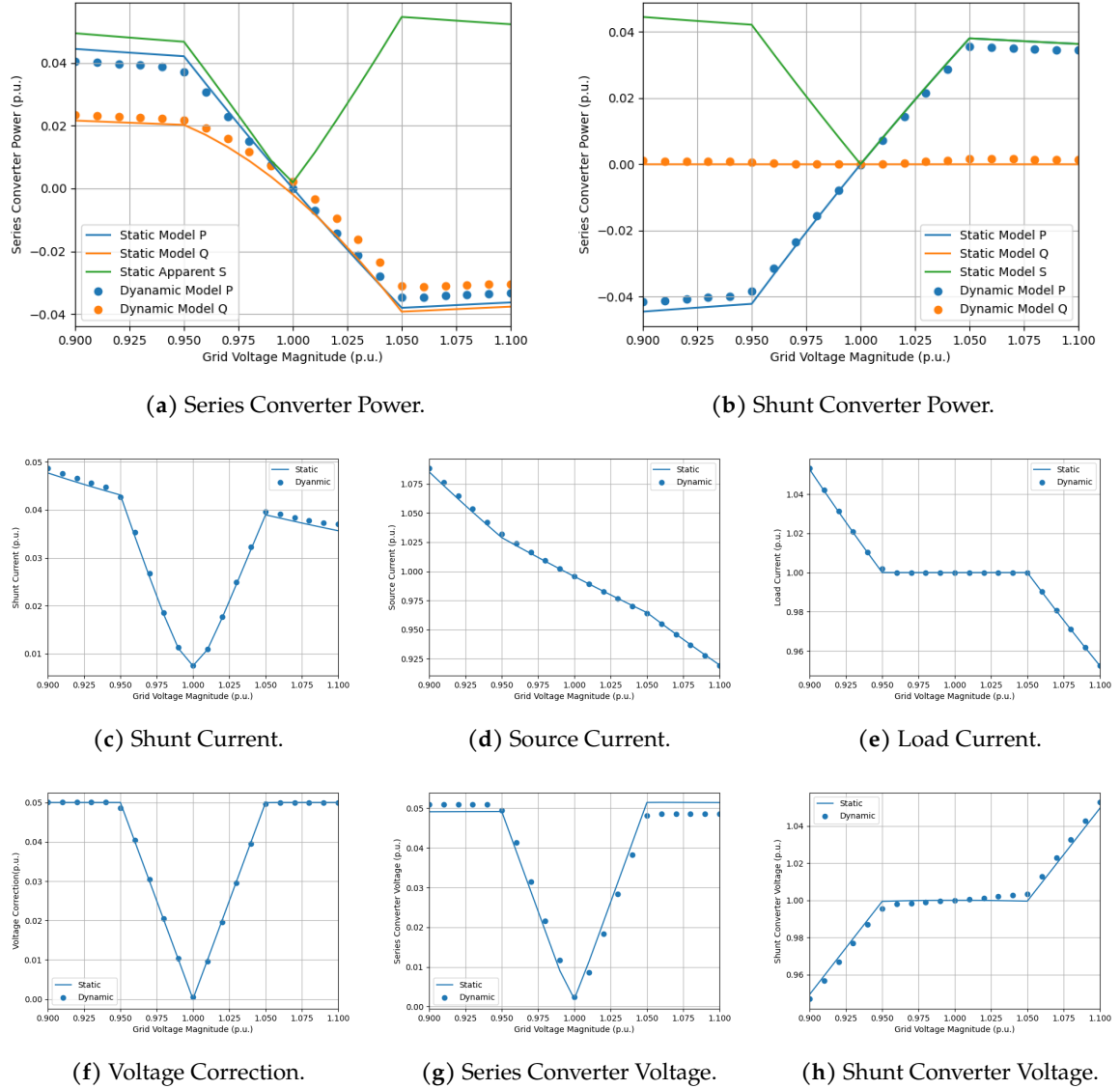


Figure 5.13: Static Model Validation with a Voltage Limit of 0.05 p.u., an Inductive Load Power Factor $\text{pf}=0.8$ and Transformer Ratio of $N_T=20$.

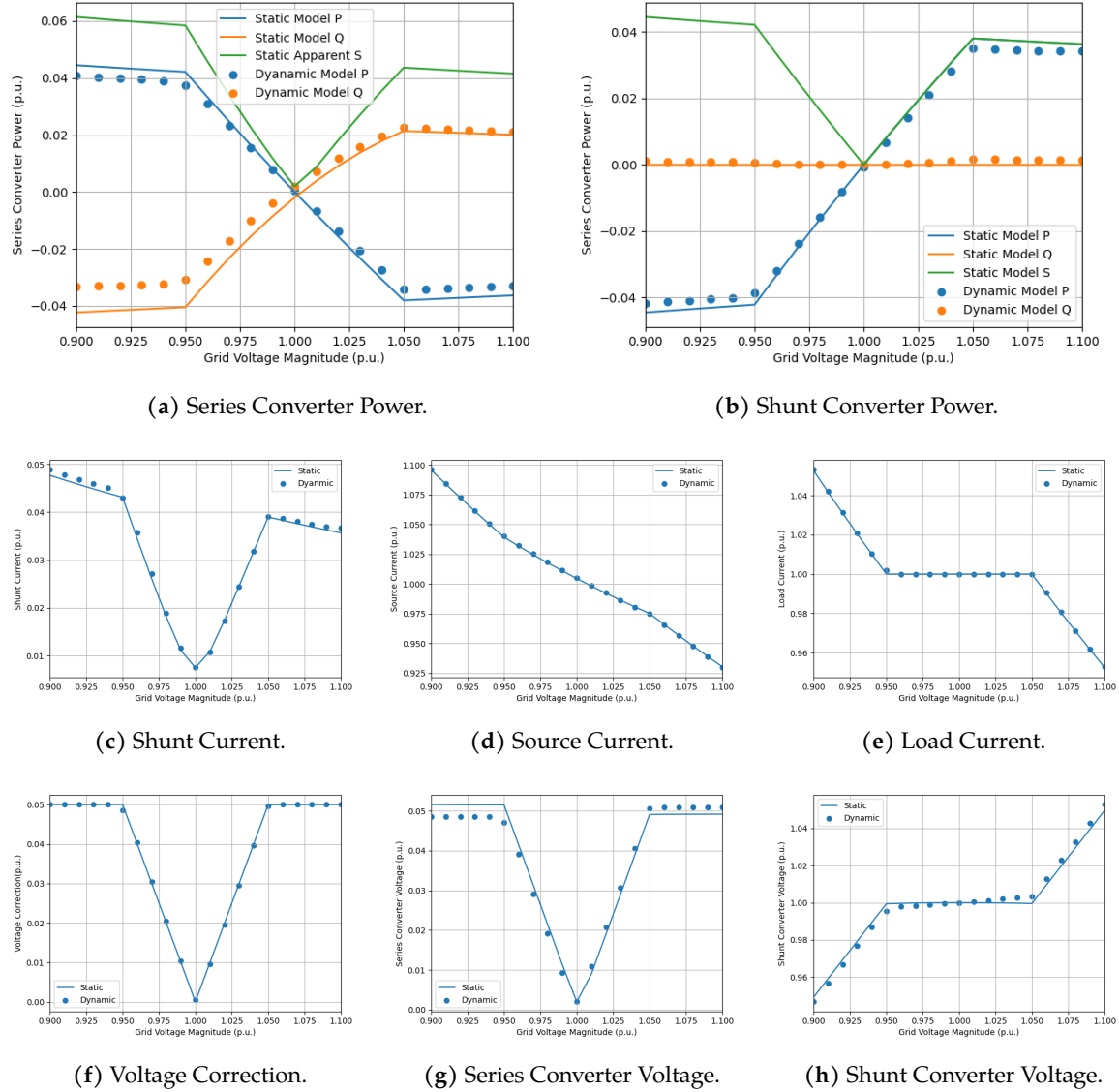


Figure 5.14: Static Model Validation with a Voltage Limit of 0.05 p.u., a Capacitive Load Power Factor $\text{pf}=0.8$ and Transformer Ratio of $N_T=20$.

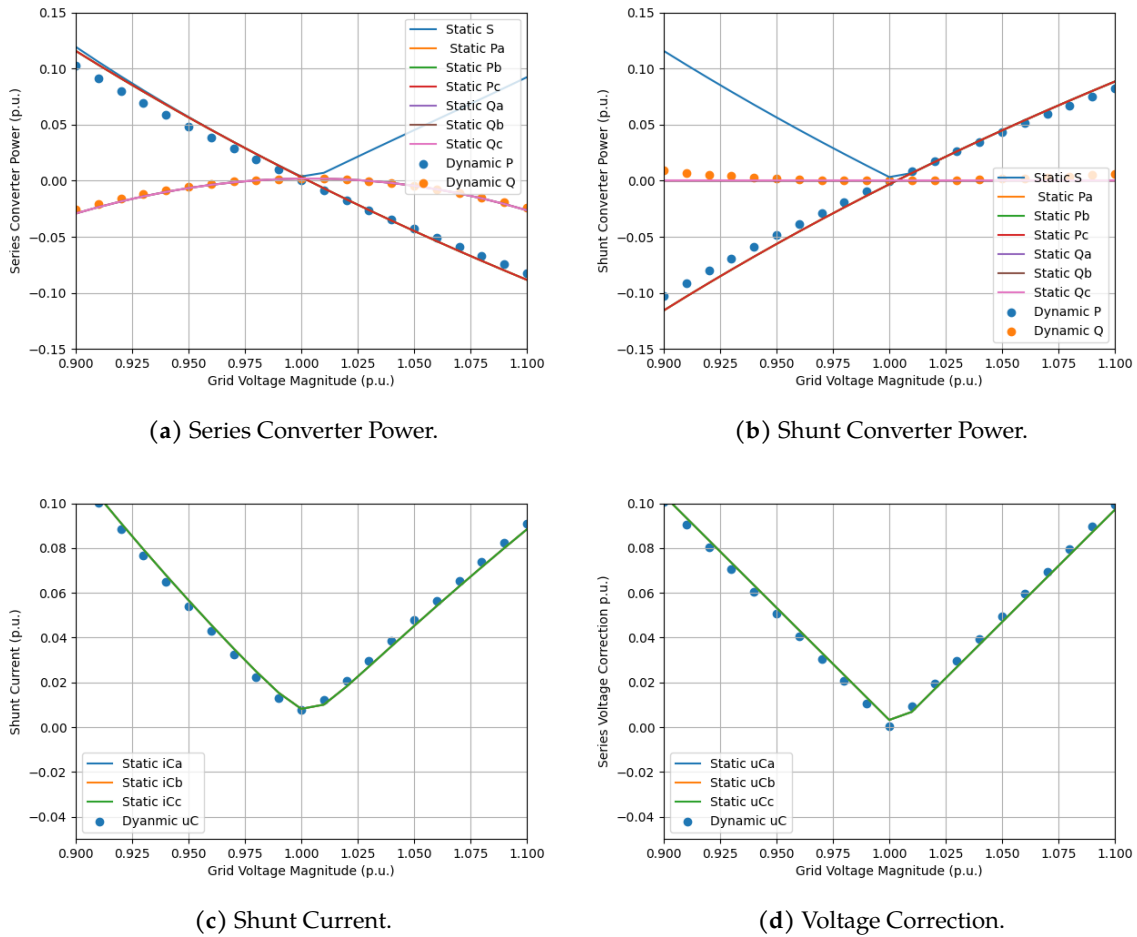


Figure 5.15: Three Phase Static Model Validation with a Load Power Factor $\text{pf}=1$ and Transformer Ratio $N_T=20$.

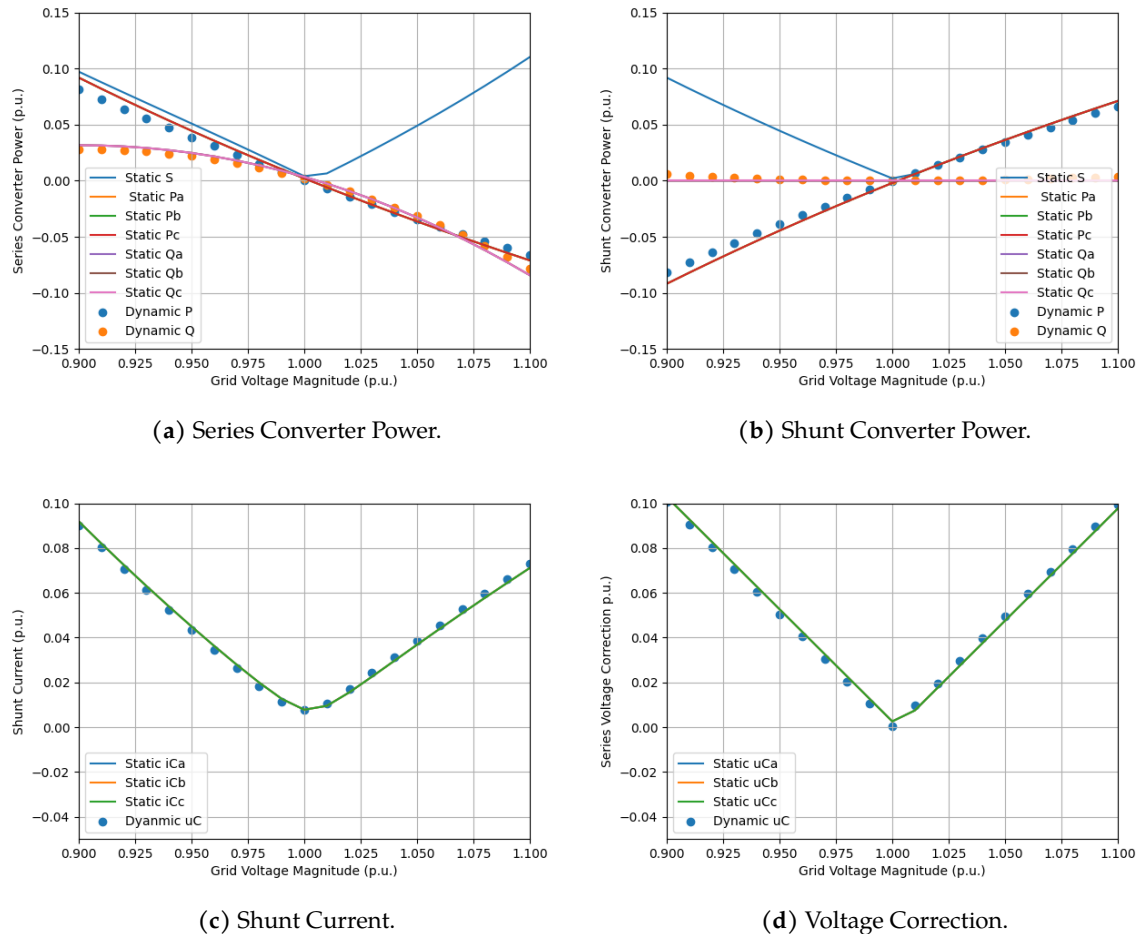


Figure 5.16: Three Phase Static Model Validation with an Inductive Load Power Factor $\text{pf}=0.8$ and Transformer Ratio of $N_T=20$.

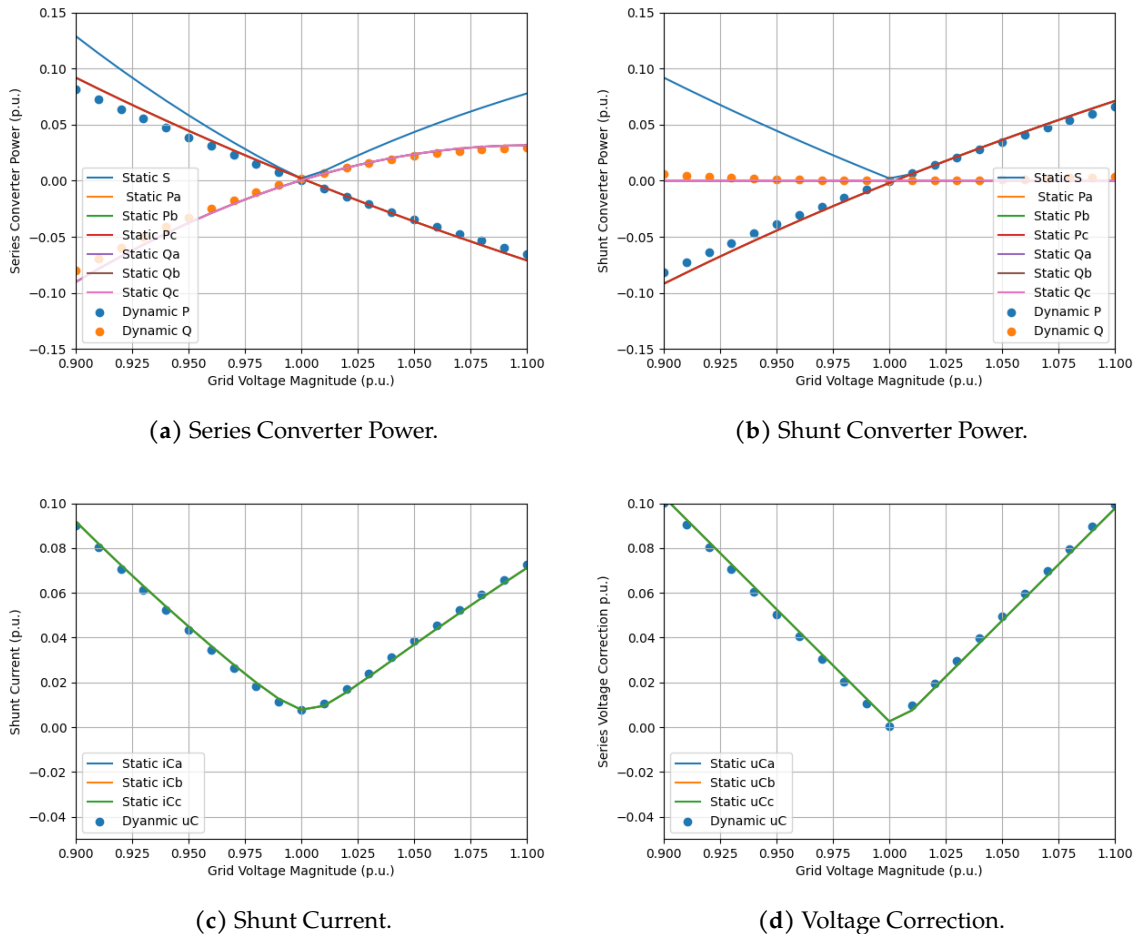
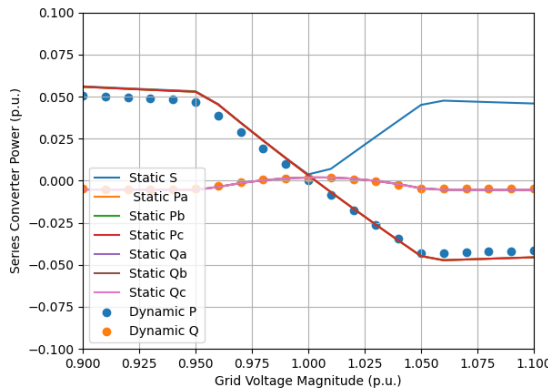
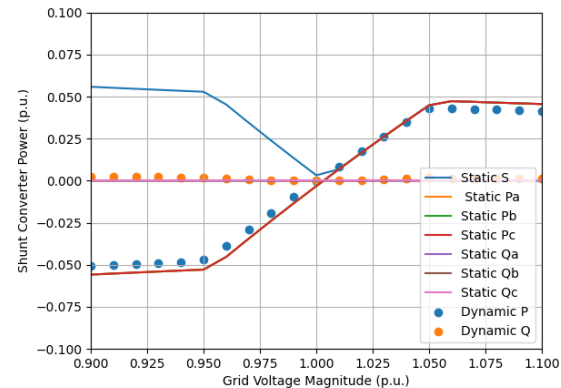


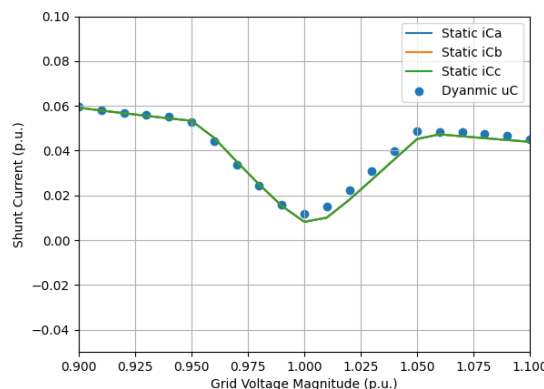
Figure 5.17: Three Phase Static Model Validation with a Capacitive Load Power Factor $\text{pf}=0.8$ and Transformer Ratio $N_T=20$.



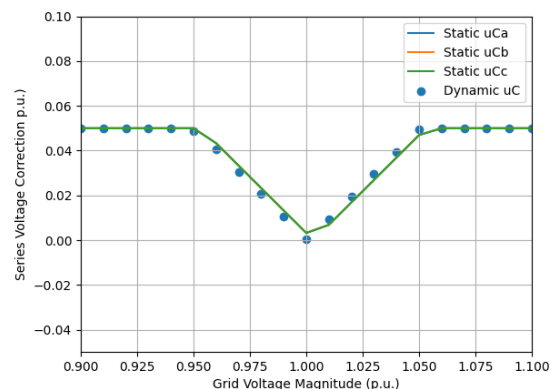
(a) Series Converter Power.



(b) Shunt Converter Power.



(c) Shunt Current.



(d) Voltage Correction.

Figure 5.18: Three Phase Static Model Validation with a Voltage Limit of 0.05p.u., Load Power Factor pf=1 and Transformer Ratio $N_T=20$.

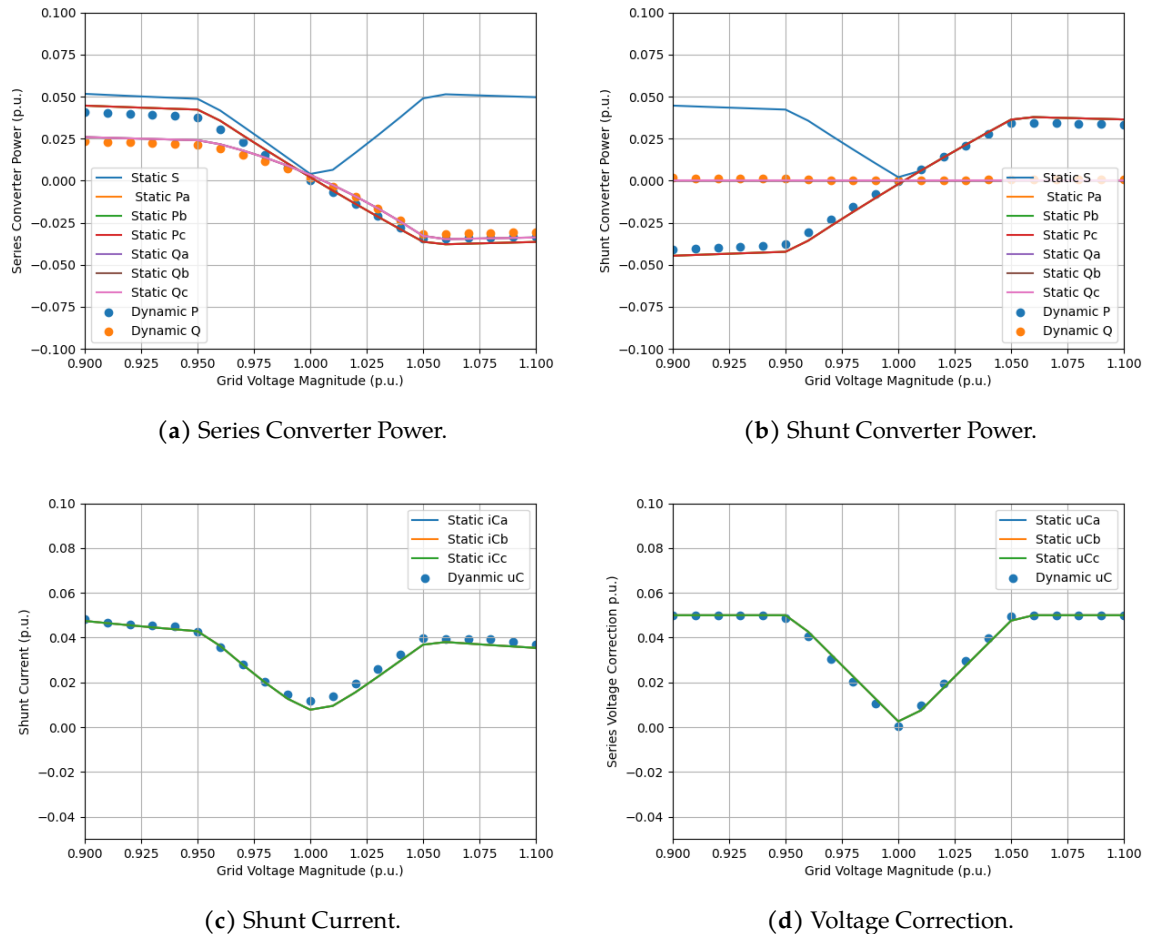


Figure 5.19: Three Phase Static Model Validation with a Voltage Limit of 0.05p.u., an Inductive Load Power Factor pf=0.8 and Transformer Ratio of $N_T=20$.

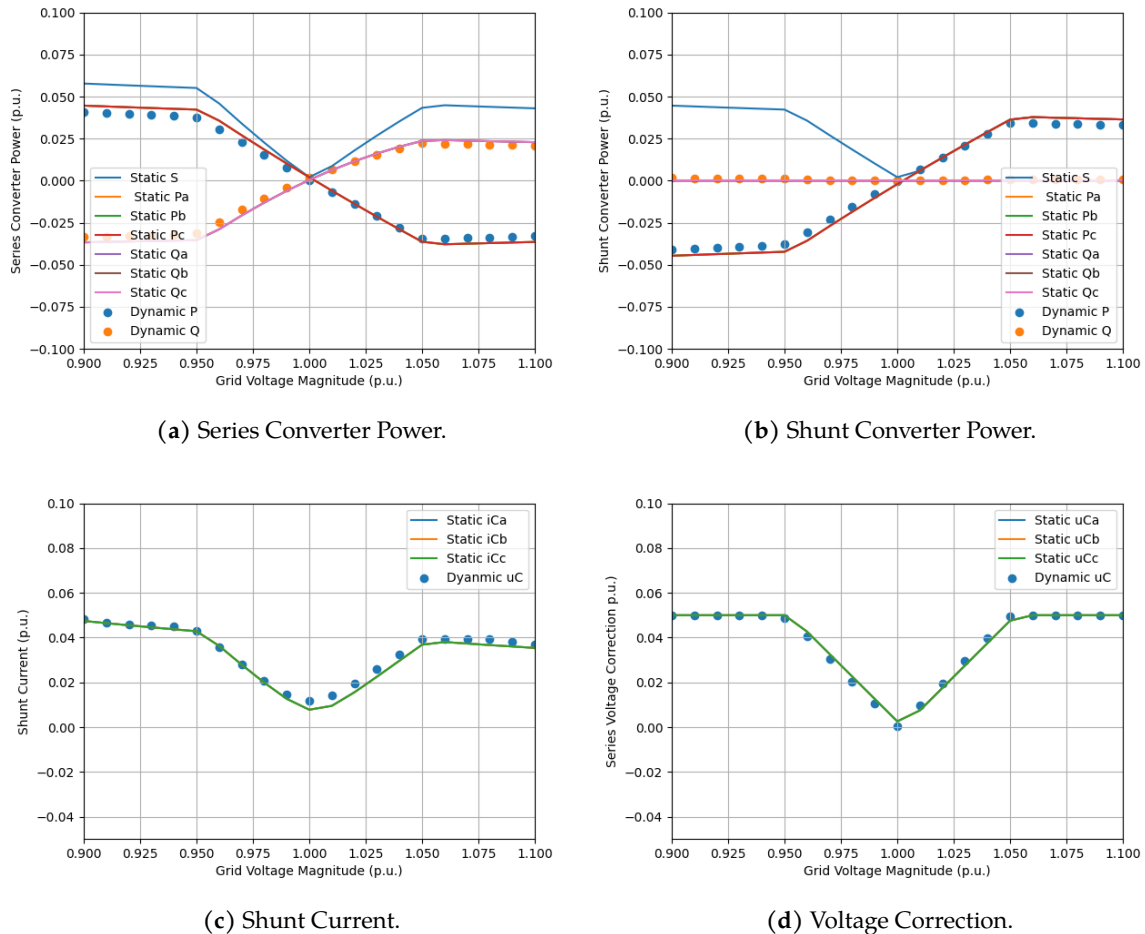


Figure 5.20: Three Phase Static Model Validation with a Voltage Limit of 0.05 p.u., a Capacitive Load Power Factor $\text{pf}=0.8$ and transformer ratio $N_T=20$.

6 Design and Results

6.1 Design Decisions

In this chapter, a sample process for designing the converter using the developed tools is shown. The filter sizing, while an important portion of this process, does not require any of these tools. Instead, it relies on the switching frequency desired at the converter. The dynamic model is used primarily for the DC link capacitor sizing, as the condition for the DC link is a dynamic variation of less than a given percentage of the DC link voltage. The static model is then used to determine both the series transformer turn ratio and the power rating of the series and shunt converters. For this process, the sample system established in Chapter 2 will be used. This system has a rated load power of 200MVA and a rated line-to-line voltage of 400 V. The desired switching frequency specified by Teknocea for the series and shunt converter is 2.5 kHz.

6.1.1 Filter Sizing

The choice was made in this application to use a simple LC filter. As such, the cutoff frequency of the filter is chosen to be 500 Hz, which is 5 times lower than the switching frequency. Using the relationship given in (6.1), and paying attention to keep the filter inductance relatively low. The filter inductance is found to be 3 mH and the filter capacitance is found to be 30 μF .

$$f_c = \frac{1}{2\pi\sqrt{LC}} \quad (6.1)$$

6.1.2 DC Link Capacitor Sizing

It is important to size the DC link capacitor close to the smallest quantity it can be as it is one of the most expensive components of the UPQC. As stated, the DC link capacitor is sized using the dynamic model. Another option would be to obtain a direct relationship between sizing of the series and shunt converters in terms of active power and the DC link capacitor sizing. However, this is beyond the scope of this project. In this design, it is assumed the DC link stability requirement is of 5% deviation from the nominal. A DC link capacitor of 10 μF would provide a variation of 3.5%, which is quite close to the requirement. As such a capacitor of 10 μF is chosen for the DC link capacitor.

6.1.3 Transformer Turns Ratio

The transformer turns ratio is chosen using the single-phase static model. The single-phase model may be used because the maximum power that can be obtained for a given voltage limit occurs during a balanced three-phase voltage correction with each phase correcting exactly the voltage limit. In this portion, the goal is to obtain a similar behavior to the static system with

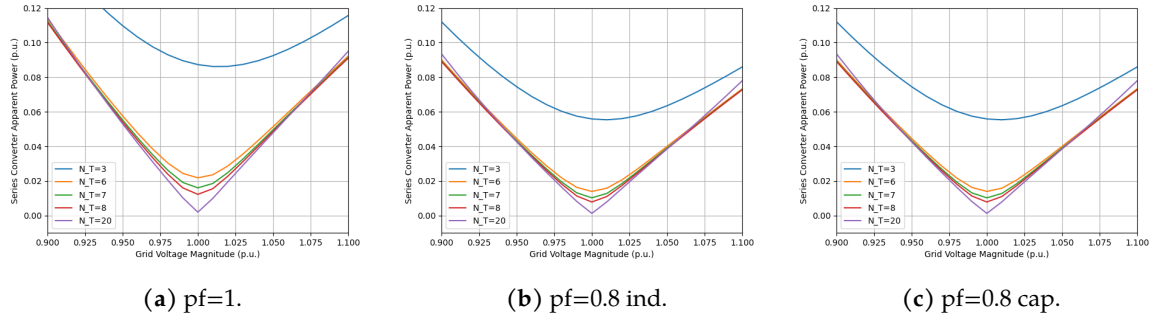


Figure 6.1: Series Apparent Power with Sweep of Transformer Ratios and Three Different Load Power Factors.

a turns ratio of 20 between 0.95 p.u. and 0.975 p.u. and between 1.025 p.u. and 1.05 p.u.. The lowest transformer ratio that gives this behavior for all three power factors is a turns ratio of 7. As such, this is the ratio chosen for this application. Sweeps of the series converter apparent power aiding in this decision are shown in Fig. 6.1.

6.1.4 Series and Shunt Converter Sizing

For the three different scenarios, the series converter apparent power is computed using the single-phase static model, as once again the worst case scenario for power will be when all the converters are correcting at maximum voltage. The results for every line of the rated series converter power extracted from the static model are shown in Fig. 6.1

Line	$u_{c,lim}$ %	99.9%		99%		95%	
		$u_{c,lim}$	$S_{cs,rat}$	$u_{c,lim}$	$S_{cs,rat}$	$u_{c,lim}$	$S_{cs,rat}$
1	0.0492	0.0612	0.0405	0.0524	0.0323	0.0442	
2	0.0488	0.0607	0.0401	0.0519	0.0323	0.0442	
3	0.0488	0.0607	0.0401	0.0519	0.0323	0.0442	
4	0.0488	0.0607	0.0401	0.0519	0.0319	0.0438	
5	0.0492	0.0612	0.0405	0.0524	0.0323	0.0442	
6	0.0492	0.0612	0.0405	0.0524	0.0323	0.0442	
7	0.0488	0.0607	0.0401	0.0519	0.0323	0.0442	

Table 6.1: Test Voltage Limits for Each Sample System Line and Corresponding Converter Power.

6.2 Results with Sample System

In order to illustrate the behavior of the converter during a day in the distribution system. Two days at opposite portions of the year are chosen, the 1st of May 2023 and 1st of November 2022.

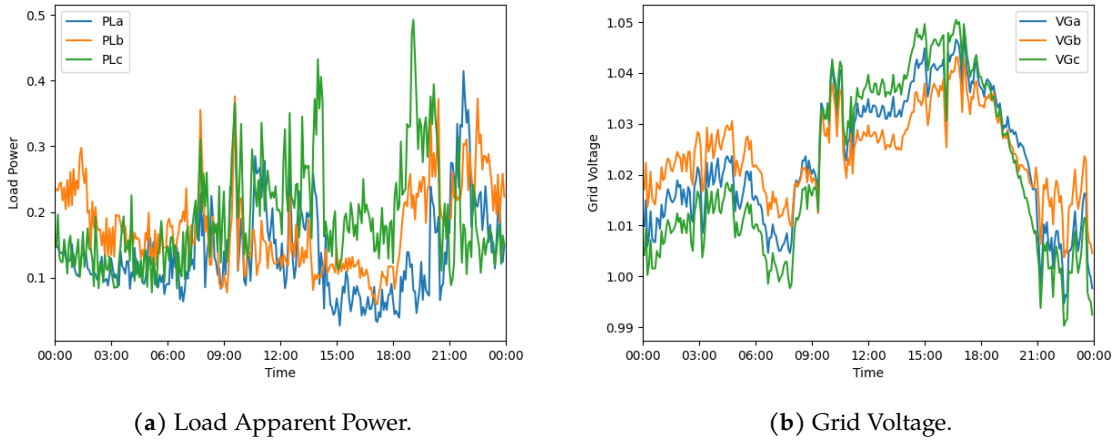


Figure 6.2: Sample Day in May for Line 1 of the Studied System.

This is necessary to account for seasonal differences in the load profile. The three voltage limit scenarios, 99.9%, 99%, and 95%, are used in both cases.

The first day investigated is the May date. The grid voltage and load power for this scenario are shown in Fig. 6.2. Since the data does not specify the power factor of the load, it will be assumed that the load has unity power factor for these simulations. The first voltage limit scenario is shown in Fig. 6.3. As this scenario is expected to correct 99.9% of all voltage deviations back to 1p.u., it is quite unlikely the load voltage will change in this scenario. Indeed in Fig. 6.3e, the load voltage remains essentially unchanged. As such, the UPQC never reaches its voltage limit. In the second voltage limit scenario, the converter hit the voltage limit in parts of the day, especially between 15h and 18h. Interestingly, although the converter does reach the voltage limit in the second scenario, there is no visible difference between the power profiles for scenarios 1 and 2, as evidenced in Figs. 6.3a&6.3b and Figs. 6.4a&6.4b.

Finally, the third scenario more obviously reaches the voltage limit. Indeed, the load voltage spends just under half of the sample day away from its nominal value in at least one phase. In addition, during this portion of the day, there is a significant difference between the power of the series and shunt converters relative to the previous two scenarios, as can be seen in Figs. 6.5a&6.5b.

The second sample day has much less voltage variation relative to the first one. Because of this smaller voltage variation, the first scenario does not reach the voltage limit, and the second scenario also barely reaches it. Even in the third scenario, there is much less variation in the load voltage relative to the other date. As such, it is quite difficult to tell the difference in the power profiles even with the third voltage limit scenario.

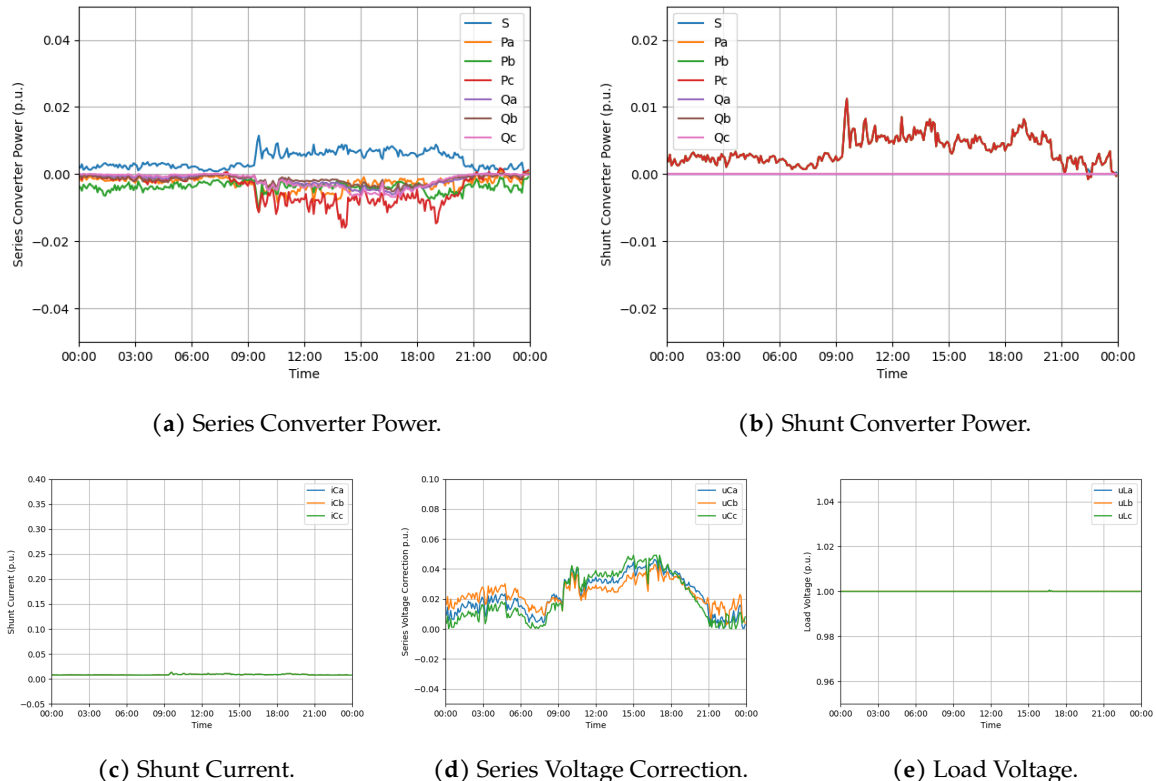


Figure 6.3: Sample Day of the UPQC Static Model from a Day in May with Voltage Limit Set to 99.9% Case.

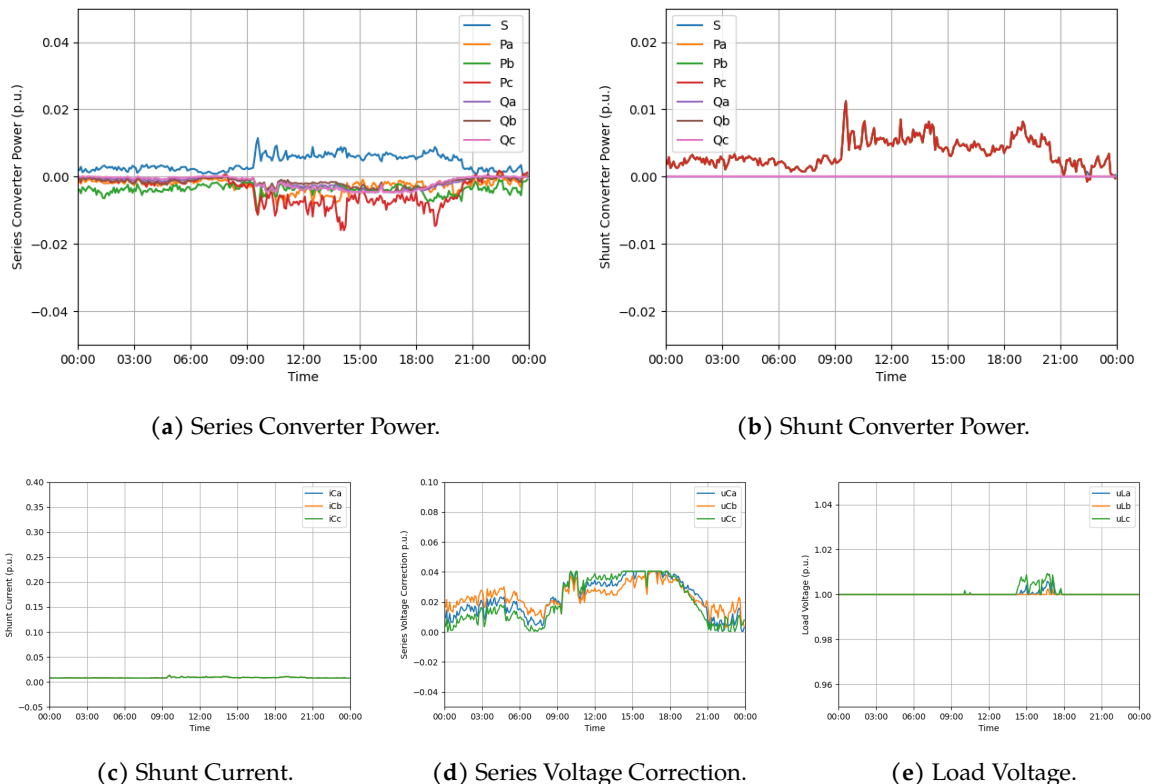


Figure 6.4: Sample Day of the UPQC Static Model from a Day in May with Voltage Limit Set to 99% Case.

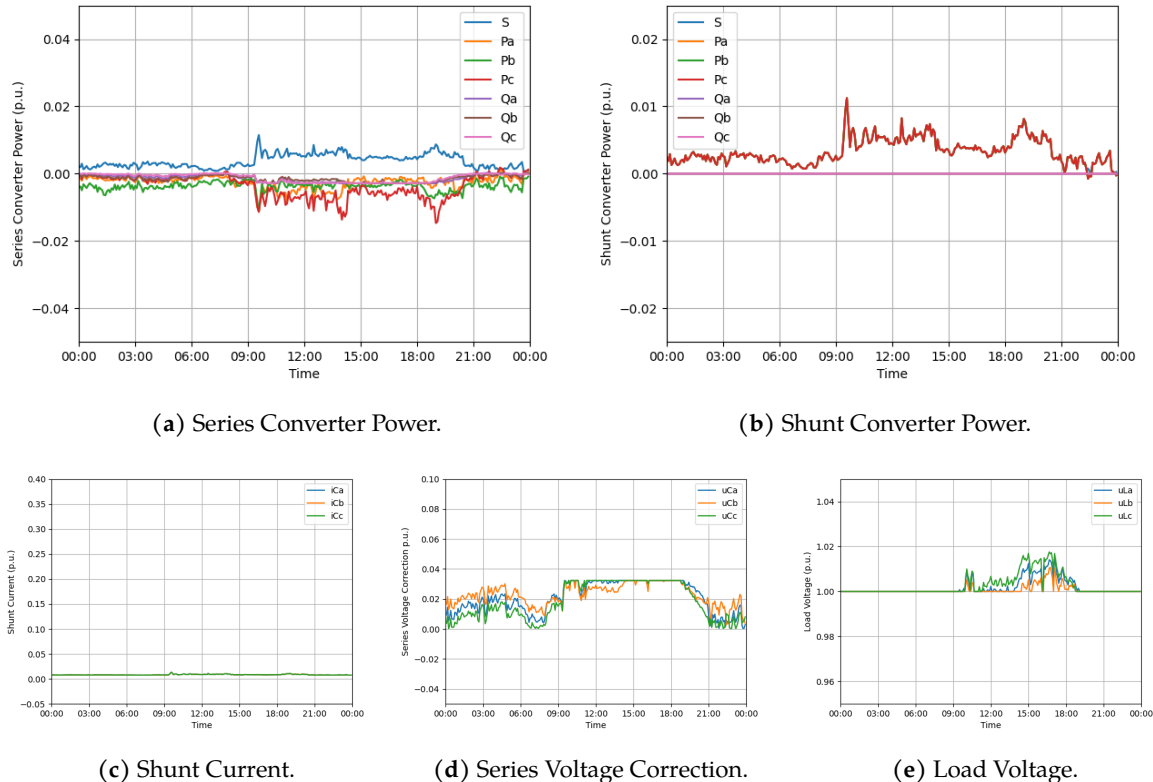


Figure 6.5: Sample Day of the UPQC Static Model from a Day in May with Voltage Limit Set to 95% Case.

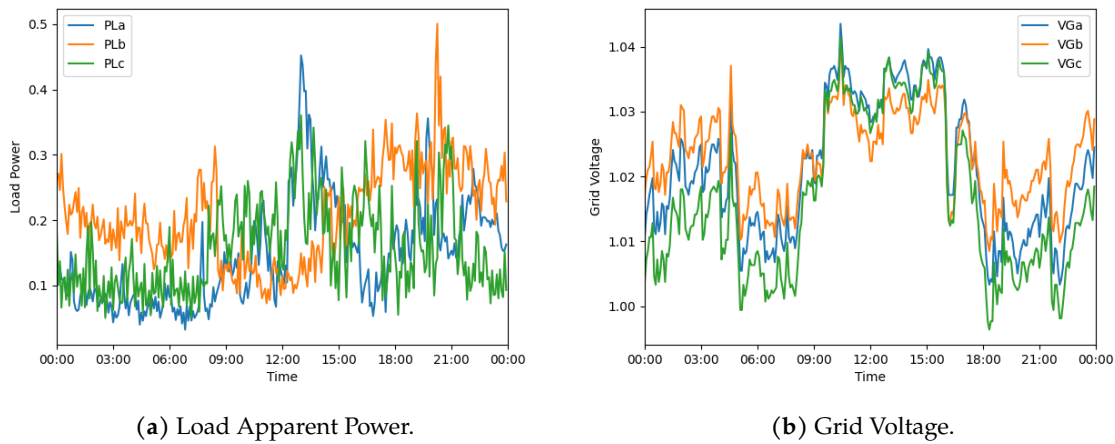


Figure 6.6: Sample Day in November for Line 1 of the Studied System.

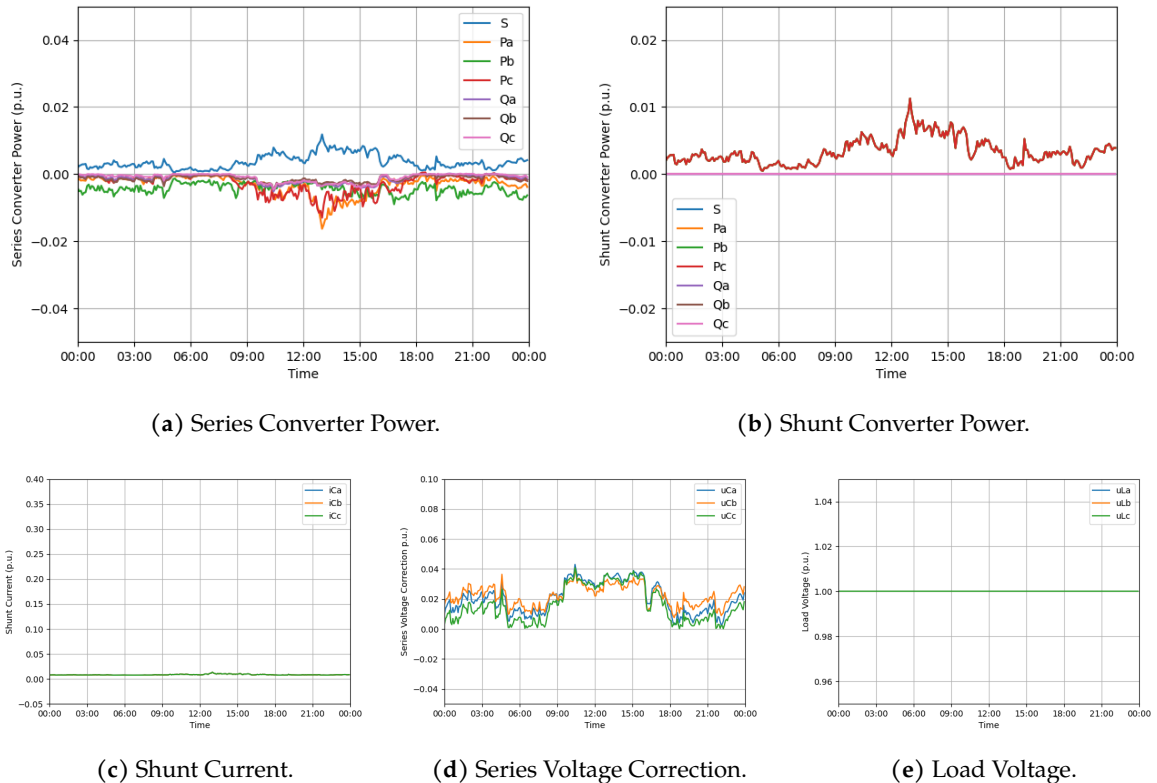


Figure 6.7: Sample Day of the UPQC Static Model from a Day in November with Voltage Limit Set to 99.9% Case.

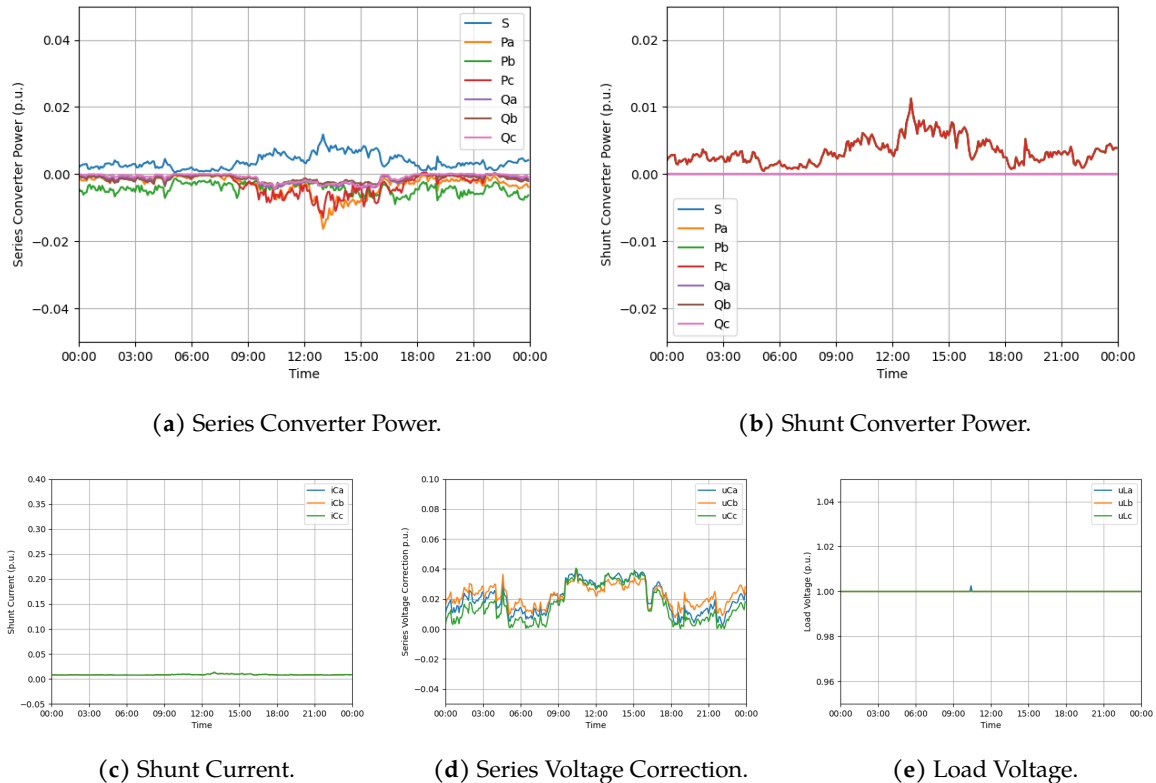


Figure 6.8: Sample Day of the UPQC Static Model from a Day in November with Voltage Limit Set to 99% Case.

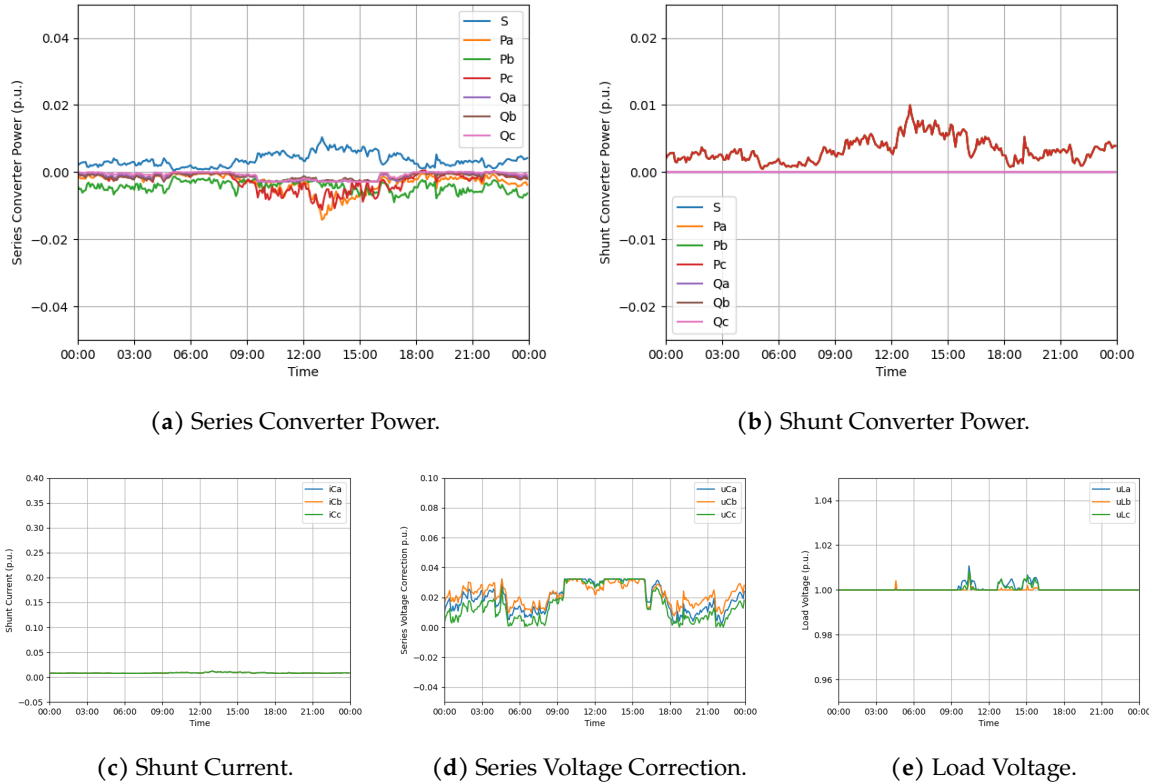


Figure 6.9: Sample Day of the UPQC Static Model from a Day in November with Voltage Limit Set to 95% Case.

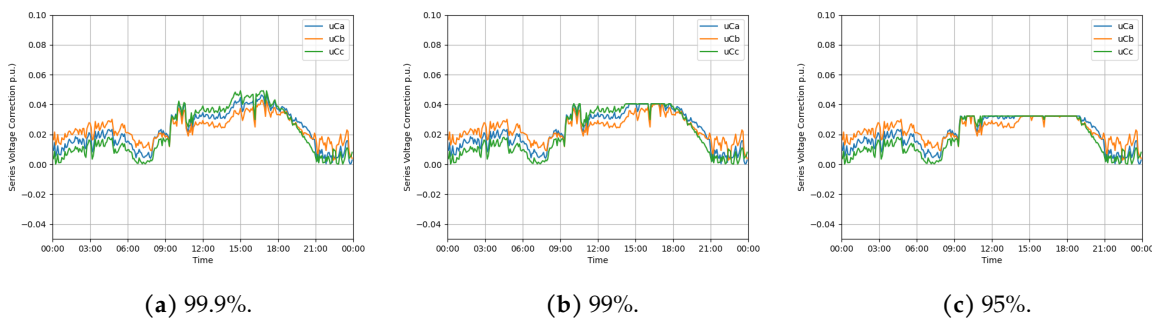


Figure 6.10: Sample Day of the UPQC Static Model from a Day in November with Voltage Limit Set to 95% Case.

7 Conclusion

The thesis has covered the development of tools for and the design process itself of a UPQC. This chapter summarizes the main contributions of the work and potentially rewarding ideas to further develop in the future.

7.1 Contributions

The most relevant findings, organized by chapter, are the following:

- Chapter 3 presents a control approach for the UPQC involving the use of the SOGI. This control approach has the primary goal of providing voltage support at the minimum power output. It is part of the larger approach to minimize the size of power electronics grid support devices to allow them to compete price-wise with the traditional approaches. In Chapter 5, it was confirmed that the controller completed the objectives set out for it.
- Chapter 4 presents an equivalent static representation of the UPQC including its filters. This equivalent representation is based on a simplification of the UPQC circuit and some assumptions about the behaviour of the controllers. In Chapter 5, it was shown that this model follows the general trend set by the dynamic model but does not replicate the behavior exactly. Despite this, it serves as a useful tool since the maximum error is 1%, which is quite low.
- Chapter 6 uses the tools above to lay out a clear design process for different components in the UPQC. This process is completed using real grid data from a Spanish DSO. Additionally, sample daily behavior graphs are displayed to showcase the standard behavior of the UPQC in the grid.

It has to be mentioned that all results, except for the dynamic simulations, have been generated with custom Python codes. The dynamic simulations were completed in Simulink.

7.2 Future work

There are many opportunities for this work to continue. In fact, Teknocea plans to leverage this work by installing an actual device in the sample grid the data is collected from. However, academically the subject also has avenues still to explore. In particular, three major possibilities attract attention:

- As stated in the paper, the shunt controller current calculation is slightly suboptimal. As the shunt converter voltage is approximated to be the converter voltage. Finding a way to obtain this value without creating instability in the system would greatly improve the behavior of the dynamic model. It might also cause the static and dynamic models to

harmonize better.

- The possibility of extending the static model to state space poses many interesting possibilities. This would allow testing of control strategies on the static model to be conducted as well. This is quite feasible as almost all the equations of the circuit are linear, except the power assumptions and the DC link. As such, the most difficult condition to respect in this case would be the DC link condition, but it could be linearized to alleviate this concern.
- The possibility of creating a voltage limit condition dependent on the load is also a possibility. It could allow the UPQC to correct greater voltage drops when the load has low demand. This way, it would maximize the available power in the converter.

Acknowledgments

Many people contributed to the completion of this project and the journey to and I would like to take the time in this portion to thank them.

First of all, I would like to thank my supervisor Oriol for providing some critical feedback and insight throughout the process of completing this project.

I would also like to thank my colleagues at eRoots. To Josep for pulling me out various times when I got stuck and for providing feedback especially in the report. To Leo for helping get the ball rolling for the project and always making himself available to answer any question that came up. To Jana for helping me believe in myself over the course of the project. I hope this is just the beginning of a long and fruitful collaboration.

Enfin je voudrais remercier ma famille. Mon père et ma mère qui ont toujours eu confiance en moi et qui m'ont poussé à poursuivre mes passions. Et à Erwan, Faustine et Zacharie, qui me poussent par leurs succès mais sont toujours là pour me décontracter et me faire rire.

A Environmental, Social, and Gender Impact

The present chapter considers the environmental impact of the integration of UPQCs in the electrical grid. This is not an easy task as many specific cases could be analyzed in different countries with different geographical situations. Instead, a generic overview of some effects is given.

A.1 Integration of Renewable Energy and Removal of Fossil Fuel Generators

The presence of the UPQC in the power grid with this application is primarily geared towards allowing more distribution level PV to be installed while minimizing disturbance to the system. This extra integration of renewable energy with stability guaranteed in the grid will allow the gradual phasing out of fossil fuel generation. This has clear environmental benefits in reducing the emission of greenhouse gases and reducing air pollution.

A.2 Social Impact of Outage Prevention

By aiding in voltage regulation, UPQCs reduce the stress on the insulation in the grid and could thus contribute to reducing faults caused by the failure of insulation. Outages have various harmful effects on society. Firstly, they can be harmful to the health of affected populations. One example is that during outages, carbon monoxide poisoning victims from unsafe use of generators increases significantly [47, 48]. Hospitalizations due to food poisoning also greatly increase due to people not disposing of food perished during the outage. Additionally, for longer outages, mental health of affected populations has shown deterioration, with reports of anxiety, depression, and even PTSD reported. Children, second language speakers, minorities, rural populations, and healthcare workers have been shown to be especially vulnerable to these health effects [48]. Secondly, crime has been shown to increase during outages, especially in areas of low economic opportunity [48]. Overall, the UPQC could provide more energy security to DSO customers which can have positive effects.

B Time Planning

Figure B.1 shows the temporal evolution of the various tasks that have constituted the project.

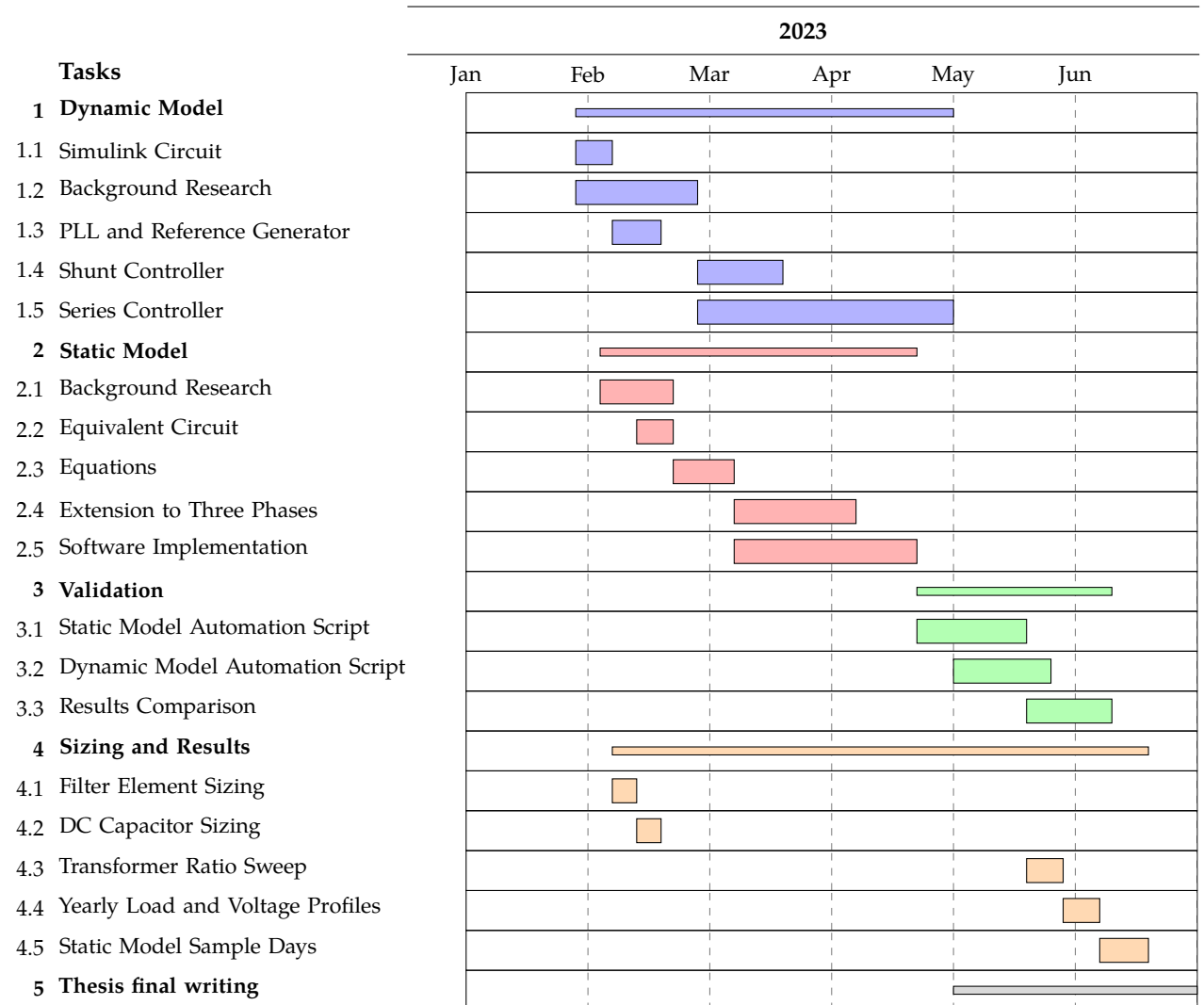


Figure B.1: Gantt Diagram Illustrating the Project Evolution.

C Budget

C.1 Equipment

The costs of machinery and digital tools required in the project development appear in Table C.1.

Table C.1: Equipment Costs.

Concept	Unit cost (€)	Quantity	Total (€)
Personal computer	1000.00	1	1000.00
Matlab individual annual license	2000.00	1	2000.00
Total			3000.00

C.2 Human resources

The working hours spent on the thesis and related work are captured in Table C.2. It also includes the cost linked to the supervision process.

Table C.2: Human Resources Costs.

Concept	Unit cost (€/h)	Quantity (h)	Total (€)
Research	25.00	100	2500.00
Code development	25.00	400	10000.00
Testing	25.00	150	3750.00
Writing	25.00	100	2500.00
Supervision	30.00	50	1500.00
Total			20250.00

C.3 Total budget

The total budget formed by aggregating equipment and human resources is shown in Table C.3. No Value Added Tax (VAT) is considered in the budget.

Table C.3: Total Budget of the Thesis.

Concept	Total (€)
Equipment	3000.00
Human resources	20250.00
Total	23250.00

2nd of July, 2023

Titouan Delorme

Bibliography

- [1] M. Allen *et al.*, "Technical summary: Global warming of 1.5 c. an ipcc special report on the impacts of global warming of 1.5 c above pre-industrial levels and related global greenhouse gas emission pathways, in the context of strengthening the global response to the threat of climate change, sustainable development, and efforts to eradicate poverty," 2019.
- [2] D. UNFCCC, "1/cp. 21,'adoption of the paris agreement'(29 january 2016), un doc fccc," CP/2015/10/Add. 1, Annex (Paris Agreement). Transatlantic Investment and ..., Tech. Rep., 2015.
- [3] O. Cf, "Transforming our world: The 2030 agenda for sustainable development," *United Nations: New York, NY, USA*, 2015.
- [4] D. Laslett, C. Carter, C. Creagh, and P. Jennings, "A large-scale renewable electricity supply system by 2030: Solar, wind, energy efficiency, storage and inertia for the south west interconnected system (swis) in western australia," *Renewable Energy*, vol. 113, pp. 713–731, 2017, issn: 0960-1481. doi: <https://doi.org/10.1016/j.renene.2017.06.023>. [Online]. Available: <https://www.sciencedirect.com/science/article/pii/S0960148117305244>.
- [5] J. R. Aguero, E. Takayesu, D. Novosel, and R. Masiello, "Modernizing the grid: Challenges and opportunities for a sustainable future," *IEEE Power and Energy Magazine*, vol. 15, no. 3, pp. 74–83, 2017. doi: <10.1109/MPE.2017.2660819>.
- [6] S. Rahman, H. Aburub, M. Moghaddami, and A. I. Sarwat, "Reverse power flow protection in grid connected pv systems," in *SoutheastCon 2018*, 2018, pp. 1–5. doi: <10.1109/SECON.2018.8478882>.
- [7] J. von Appen, M. Braun, T. Stetz, K. Diwold, and D. Geibel, "Time in the sun: The challenge of high pv penetration in the german electric grid," *IEEE Power and Energy Magazine*, vol. 11, no. 2, pp. 55–64, 2013. doi: <10.1109/MPE.2012.2234407>.
- [8] V. Telukunta, J. Pradhan, A. Agrawal, M. Singh, and S. G. Srivani, "Protection challenges under bulk penetration of renewable energy resources in power systems: A review," *CSEE Journal of Power and Energy Systems*, vol. 3, no. 4, pp. 365–379, 2017. doi: <10.17775/CSEEJPES.2017.00030>.
- [9] M. M. Haque and P. Wolfs, "A review of high pv penetrations in lv distribution networks: Present status, impacts and mitigation measures," *Renewable and Sustainable Energy Reviews*, vol. 62, pp. 1195–1208, 2016, issn: 1364-0321. doi: <https://doi.org/10.1016/j.rser.2016.04.025>. [Online]. Available: <https://www.sciencedirect.com/science/article/pii/S1364032116300429>.
- [10] F. C. L. Trindade, T. S. D. Ferreira, M. G. Lopes, and W. Freitas, "Mitigation of fast voltage variations during cloud transients in distribution systems with pv solar farms," *IEEE Transactions on Power Delivery*, vol. 32, no. 2, pp. 921–932, 2017. doi: <10.1109/TPWRD.2016.2562922>.

- [11] Y. Hou, M. Z. Liu, and L. F. Ochoa, "Residential pv hosting capacity, voltage unbalance, and power rebalancing: An australian case study," in *2022 IEEE PES Innovative Smart Grid Technologies Conference Europe (ISGT-Europe)*, 2022, pp. 1–5. doi: [10.1109/ISGT-Europe54678.2022.9960503](https://doi.org/10.1109/ISGT-Europe54678.2022.9960503).
- [12] K. DSouza, Y. Wang, G. Cakir, M. Baran, and T. Zhao, "Power electronics assisted voltage regulator: An effective solution for mitigating voltage variations caused by high penetration pv on a distribution system," in *2021 IEEE 12th International Symposium on Power Electronics for Distributed Generation Systems (PEDG)*, 2021, pp. 1–5. doi: [10.1109/PEDG51384.2021.9494246](https://doi.org/10.1109/PEDG51384.2021.9494246).
- [13] H. Ghoddami and A. Yazdani, "A mitigation strategy for temporary overvoltages caused by grid-connected photovoltaic systems," *IEEE Transactions on Energy Conversion*, vol. 30, no. 2, pp. 413–420, 2015. doi: [10.1109/TEC.2014.2364033](https://doi.org/10.1109/TEC.2014.2364033).
- [14] M. Krarti, "Chapter 4 - utility rate structures and grid integration," in *Optimal Design and Retrofit of Energy Efficient Buildings, Communities, and Urban Centers*, M. Krarti, Ed., Butterworth-Heinemann, 2018, pp. 189–245, ISBN: 978-0-12-849869-9. doi: <https://doi.org/10.1016/B978-0-12-849869-9.00004-1>. [Online]. Available: <https://www.sciencedirect.com/science/article/pii/B9780128498699000041>.
- [15] P. Murty, "Chapter 11 - overvoltages," in *Electrical Power Systems*, P. Murty, Ed., Boston: Butterworth-Heinemann, 2017, pp. 229–257, ISBN: 978-0-08-101124-9. doi: <https://doi.org/10.1016/B978-0-08-101124-9.00011-5>. [Online]. Available: <https://www.sciencedirect.com/science/article/pii/B9780081011249000115>.
- [16] F. Chiang, "Implications of temporary overvoltages for insulation coordination for equipment within low-voltage systems," in *2011 IEEE Symposium on Product Compliance Engineering Proceedings*, 2011, pp. 1–6. doi: [10.1109/PSES.2011.6088243](https://doi.org/10.1109/PSES.2011.6088243).
- [17] M. Florkowski, M. Kuniewski, J. Furgał, and P. Pajak, "Investigation of overvoltages in distribution transformers," in *2017 18th International Scientific Conference on Electric Power Engineering (EPE)*, 2017, pp. 1–4. doi: [10.1109/EPE.2017.7967288](https://doi.org/10.1109/EPE.2017.7967288).
- [18] S. Alyami, Y. Wang, C. Wang, J. Zhao, and B. Zhao, "Adaptive real power capping method for fair overvoltage regulation of distribution networks with high penetration of pv systems," *IEEE Transactions on Smart Grid*, vol. 5, no. 6, pp. 2729–2738, 2014. doi: [10.1109/TSG.2014.2330345](https://doi.org/10.1109/TSG.2014.2330345).
- [19] J. Pou, D. Boroyevich, and R. Pindado, "Effects of imbalances and nonlinear loads on the voltage balance of a neutral-point-clamped inverter," *IEEE Transactions on Power Electronics*, vol. 20, no. 1, pp. 123–131, 2005. doi: [10.1109/TPEL.2004.839823](https://doi.org/10.1109/TPEL.2004.839823).
- [20] F. J. T. E. Ferreira, J. Alberto, and A. T. de Almeida, "Voltage unbalance impact on coil-side temperature rise in a delta-connected, dual-winding induction motor," in *2020 IEEE International Conference on Industrial Technology (ICIT)*, 2020, pp. 925–930. doi: [10.1109/ICIT45562.2020.9067201](https://doi.org/10.1109/ICIT45562.2020.9067201).

- [21] X. Liu, A. Aichhorn, L. Liu, and H. Li, "Coordinated control of distributed energy storage system with tap changer transformers for voltage rise mitigation under high photovoltaic penetration," *IEEE Transactions on Smart Grid*, vol. 3, no. 2, pp. 897–906, 2012. doi: [10.1109/TSG.2011.2177501](https://doi.org/10.1109/TSG.2011.2177501).
- [22] A. Szultka, S. Szultka, S. Czapp, and R. Zajczyk, "Voltage variations and their reduction in a rural low-voltage network with pv sources of energy," *Electronics*, vol. 10, no. 14, 2021, issn: 2079-9292. doi: [10.3390/electronics10141620](https://doi.org/10.3390/electronics10141620). [Online]. Available: <https://www.mdpi.com/2079-9292/10/14/1620>.
- [23] Y. Liu, J. Bebic, B. Kroposki, J. de Bedout, and W. Ren, "Distribution system voltage performance analysis for high-penetration pv," in *2008 IEEE Energy 2030 Conference*, 2008, pp. 1–8. doi: [10.1109/ENERGY.2008.4781069](https://doi.org/10.1109/ENERGY.2008.4781069).
- [24] X. Su, M. A. S. Masoum, and P. J. Wolfs, "Optimal pv inverter reactive power control and real power curtailment to improve performance of unbalanced four-wire lv distribution networks," *IEEE Transactions on Sustainable Energy*, vol. 5, no. 3, pp. 967–977, 2014. doi: [10.1109/TSTE.2014.2313862](https://doi.org/10.1109/TSTE.2014.2313862).
- [25] S. Deshmukh, B. Natarajan, and A. Pahwa, "Voltage/var control in distribution networks via reactive power injection through distributed generators," *IEEE Transactions on Smart Grid*, vol. 3, no. 3, pp. 1226–1234, 2012, Cited by: 142. doi: [10.1109/TSG.2012.2196528](https://doi.org/10.1109/TSG.2012.2196528). [Online]. Available: <https://www.scopus.com/inward/record.uri?eid=2-s2.0-84865522374&doi=10.1109/TSG.2012.2196528&partnerID=40&md5=43863827993c1794baa56c0477faabe0>.
- [26] V. Calderaro, G. Conio, V. Galdi, G. Massa, and A. Piccolo, "Optimal decentralized voltage control for distribution systems with inverter-based distributed generators," *IEEE Transactions on Power Systems*, vol. 29, no. 1, pp. 230–241, 2014, Cited by: 200. doi: [10.1109/TPWRS.2013.2280276](https://doi.org/10.1109/TPWRS.2013.2280276). [Online]. Available: <https://www.scopus.com/inward/record.uri?eid=2-s2.0-84891558945&doi=10.1109/TPWRS.2013.2280276&partnerID=40&md5=bd915483106661eb57e5d3a9f9e4f9e2>.
- [27] B. Noone, "Pv integration on australian distribution networks," *The Australian PV Association, UNSW, Australia*, 2013.
- [28] Y. Liu, J. Bebic, B. Kroposki, J. De Bedout, and W. Ren, "Distribution system voltage performance analysis for high-penetration pv," in *2008 IEEE energy 2030 conference*, IEEE, 2008, pp. 1–8.
- [29] "Ieee standard for interconnecting distributed resources with electric power systems," *IEEE Std 1547-2003*, pp. 1–28, 2003. doi: [10.1109/IEEESTD.2003.94285](https://doi.org/10.1109/IEEESTD.2003.94285).
- [30] E. Feilat. "Power quality enhancement using custom power devices." (Apr. 2014), [Online]. Available: https://www.researchgate.net/publication/322644524_Power_Quality_Enhancement_using_Custom_Power_Devices#fullTextFileContent.

- [31] A. Ghosh, A. Jindal, and A. Joshi, "Design of a capacitor-supported dynamic voltage restorer (dvr) for unbalanced and distorted loads," *IEEE Transactions on Power Delivery*, vol. 19, no. 1, pp. 405–413, 2004. doi: [10.1109/TPWRD.2003.820198](https://doi.org/10.1109/TPWRD.2003.820198).
- [32] P. Wolfs and A. Maung Than Oo, "Improvements to lv distribution system pv penetration limits using a dstatcom with reduced dc bus capacitance," in *2013 IEEE Power and Energy Society General Meeting*, 2013, pp. 1–5. doi: [10.1109/PESMG.2013.6672294](https://doi.org/10.1109/PESMG.2013.6672294).
- [33] C.-S. Chen, C.-H. Lin, W.-L. Hsieh, C.-T. Hsu, and T.-T. Ku, "Enhancement of pv penetration with dstatcom in taipower distribution system," *IEEE Transactions on Power Systems*, vol. 28, no. 2, pp. 1560–1567, 2013. doi: [10.1109/TPWRS.2012.2226063](https://doi.org/10.1109/TPWRS.2012.2226063).
- [34] F. Shahnia, A. Ghosh, G. Ledwich, and F. Zare, "Voltage unbalance improvement in low voltage residential feeders with rooftop pvs using custom power devices," *International Journal of Electrical Power and Energy Systems*, vol. 55, pp. 362–377, 2014, issn: 0142-0615. doi: <https://doi.org/10.1016/j.ijepes.2013.09.018>. [Online]. Available: <https://www.sciencedirect.com/science/article/pii/S0142061513004006>.
- [35] L. Gyugyi, C. Schauder, S. Williams, T. Rietman, D. Torgerson, and A. Edris, "The unified power flow controller: A new approach to power transmission control," *IEEE Transactions on Power Delivery*, vol. 10, no. 2, pp. 1085–1097, 1995. doi: [10.1109/61.400878](https://doi.org/10.1109/61.400878).
- [36] J. Dixon, L. Moran, J. Rodriguez, and R. Domke, "Reactive power compensation technologies: State-of-the-art review," *Proceedings of the IEEE*, vol. 93, no. 12, pp. 2144–2164, 2005. doi: [10.1109/JPROC.2005.859937](https://doi.org/10.1109/JPROC.2005.859937).
- [37] F. Nepsha, V. Voronin, R. Belyaevsky, V. Efremenko, and K. Varnavskiy, "Application of facts devices in power supply systems of coal mines," *E3S Web of Conferences*, vol. 174, p. 03 026, Jan. 2020. doi: [10.1051/e3sconf/202017403026](https://doi.org/10.1051/e3sconf/202017403026).
- [38] H. Zhu and J. Wang, "Research on passivity based control and active disturbance rejection control for mmc-upqc," in *IECON 2017 - 43rd Annual Conference of the IEEE Industrial Electronics Society*, 2017, pp. 6425–6430. doi: [10.1109/IECON.2017.8217119](https://doi.org/10.1109/IECON.2017.8217119).
- [39] M. Gayatri and A. M. Parimi, "Mitigation of supply and load side disturbances in an ac microgrid using upqc," in *2016 IEEE 6th International Conference on Power Systems (ICPS)*, 2016, pp. 1–6. doi: [10.1109/ICPES.2016.7584116](https://doi.org/10.1109/ICPES.2016.7584116).
- [40] C. R. Reddy, A. G. Prasad, D. C. Sekhar, B. S. Goud, K. Kumari, and M. D. Kumar, "Voltage sag and swell compensation in integrated system using advanced upqc," in *2021 International Conference on Decision Aid Sciences and Application (DASA)*, 2021, pp. 419–423. doi: [10.1109/DASA53625.2021.9682233](https://doi.org/10.1109/DASA53625.2021.9682233).
- [41] A. Agrawal, P. Agarwal, and P. Jena, "Compensation of voltage flicker using unified power quality conditioner (upqc)," in *2014 IEEE International Conference on Power Electronics, Drives and Energy Systems (PEDES)*, 2014, pp. 1–5. doi: [10.1109/PEDES.2014.7042046](https://doi.org/10.1109/PEDES.2014.7042046).
- [42] S. Kaliappan, M. Poornima, and R. Rajeswari, "Improvement of source voltage and load current harmonic mitigation using upqc: A survey," in *2013 7th International Conference on Intelligent Systems and Control (ISCO)*, 2013, pp. 110–114. doi: [10.1109/ISCO.2013.6481132](https://doi.org/10.1109/ISCO.2013.6481132).

- [43] “Chapter 11 - unified power quality conditioner (upqc),” in *Power Quality in Power Systems and Electrical Machines*, E. F. Fuchs and M. A. Masoum, Eds., Burlington: Academic Press, 2008, pp. 443–468, ISBN: 978-0-12-369536-9. doi: <https://doi.org/10.1016/B978-012369536-9.50012-7>. [Online]. Available: <https://www.sciencedirect.com/science/article/pii/B9780123695369500127>.
- [44] P. Raboni, “Modelling, control and integration of distributed generators for enhanced ancillary services,” Ph.D. dissertation, Jan. 2016. doi: [10.5278/vbn.phd.engsci.00051](https://doi.org/10.5278/vbn.phd.engsci.00051).
- [45] A. Jeraldine Viji and T. Aruldoss Albert Victoire, “Enhanced pll based srf control method for upqc with fault protection under unbalanced load conditions,” *International Journal of Electrical Power and Energy Systems*, vol. 58, pp. 319–328, 2014, ISSN: 0142-0615. doi: <https://doi.org/10.1016/j.ijepes.2014.01.039>. [Online]. Available: <https://www.sciencedirect.com/science/article/pii/S0142061514000520>.
- [46] “Grid synchronization in single-phase power converters,” in *Grid Converters for Photovoltaic and Wind Power Systems*. John Wiley and Sons, Ltd, 2011, ch. 4, pp. 43–91, ISBN: 9780470667057. doi: <https://doi.org/10.1002/9780470667057.ch4>. eprint: <https://onlinelibrary.wiley.com/doi/pdf/10.1002/9780470667057.ch4>. [Online]. Available: <https://onlinelibrary.wiley.com/doi/abs/10.1002/9780470667057.ch4>.
- [47] D. A. Call, “Changes in ice storm impacts over time: 1886–2000,” *Weather, Climate, and Society*, vol. 2, no. 1, pp. 23–35, 2010. doi: <https://doi.org/10.1175/2009WCAS1013.1>. [Online]. Available: https://journals.ametsoc.org/view/journals/wcas/2/1/2009wcas1013_1.xml.
- [48] A. Andresen, L. Kurtz, D. Hondula, S. Meerow, and M. Gall, “Understanding the social impacts of power outages in north america:a systematic review,” *Environmental Research Letters*, vol. 18, May 2023. doi: [10.1088/1748-9326/acc7b9](https://doi.org/10.1088/1748-9326/acc7b9).